ARL 68-0184

FACULTÉ DES SCIENCES DE PARIS

66649

LABORATOIRE DE PHYSIQUE DES SOLIDES

Équipe de Recherche Associée au C. N. R. S. : OPTIQUE DES SEMICONDUCTEURS

SCIENTIFIC REPORT N° 1

OPTICAL STUDIES OF LATTICE VIBRATION IN II-VI SEMICONDUCTING COMPOUNDS

M. BALKANSKI

D D C
OCT 29 1968
RECEIVED
C

GRANT N° E00AR -68-0016

SCIENTIFIC REPORT N° 1

OPTICAL STUDIES OF LATTICE VIBRATION IN II-VI SEMICONDUCTING COMPOUNDS

M. BALKANSKI

Laboratoire de Physique des Solides de la Faculté des Sciences de Paris

Equipe de Recherche Associée au C. N. R. S. : Optique des Semiconducteurs

9, Quai Saint-Bernard - Paris 5ème

OPTICAL STUDIES OF LATTICE VIBRATIONS

IN II-VI SEMICONDUCTING COMPOUNDS

M. Balkanski

Laboratoire de Physique des Solides
de la Faculté des Sciences de Paris

------

1. Introduction.

In recent years considerable efforts have been developped to-
ward the understanding of the main features of lattice dynamics of
a great number of crystals among which the II-VI semiconductor com-
pounds have a good position. Neutron scattering technics beeing in-
applicable to most of these compounds the experimental determinations
of the normal mode frequencies are essentially done by infrared spec-
trometry and Raman scattering. Being ionic crystals all these com-
pounds possess first order dipole moments due to the relative dis-
placement of the constituting ions. The optical vibrational modes
are often allowed for optical transitions in view of specific selec-
tion rules and give the possibility of direct determination of the
frequencies of these modes at the center of the Brillouin zone. Those
of the optical modes which are not allowed for direct optical transi-
tions are often allowed in Raman scattering and hence available for
direct determination by spectroscopic technics.

Normal modes frequencies at the edge of the Brillouin zone are
determined by second and higher order processes due to their partici-
pation in two or three phonon combinations as well in infrared spec-
troscopy as in Raman scattering.

The realistic boundary conditions taking into consideration the
discontinuity at the surface of the crystal bring up the surface modes
of vibrations for the normal lattice and the localized surface modes
for a crystal with foreign atoms absorbed at the surface.

Presence of imperfections or foreign atoms leads to the appear-
ance of localized modes of vibrations which are also coupled to the
radiation field by means of resonant absorption in the infrared region
and by Raman scattering.

Parallel to the experimental investigations theoretical studies have been developed and the dispersion relations calculated for same of the II-VI compounds. The theory of systems with high impurity concentration and the lattice dynamics of the alloys is now under way.

2. Crystal Structures.

The II-VI semiconducting compounds crystallize in a variety of polymorphic modifications, the principal structure types being :

a) Cubic zinc-blende (sphalerite) structure based on the cubic space group T_d^2 :

ZnS, ZnSe, ZnTe, CdTe, HgS, HgSe, HgTe crystallize preferentially in the zinc-blende structure.

Each unit cell contains 2 atoms and the crystal will therefore possess 6 phonon branches.

b) Hexagonal wurtzite (zincite) structure based on the hexagonal space group C_{6v}^4 :

ZnO, ZnS, CdS, CdSe crystallize preferentially in the wurtzite structure.

Each unit cell contains 4 atoms and the crystal will therefore possess 12 phonon branches.

A schematic representation of these two crystals crystals structures is given in Fig.1.
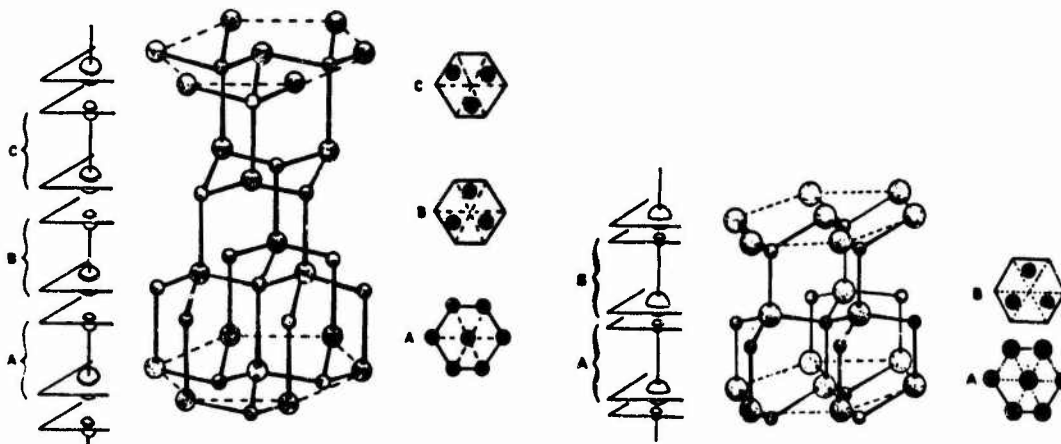
Figure 1. Schematic representation of Blende and Wurtzite crystal structures.

On the left side is shown the cubic structure where one can distinguish three different successions of layers A, B, and C, with alternating atoms. On the right side is the hexagonal structure where one finds only two different successions of layers A and B respectively.

On Fig.2 are schematized the two elementary cells containing two atoms for the cubic structure shown on the left and four atoms for the hexagonal structure on the right.
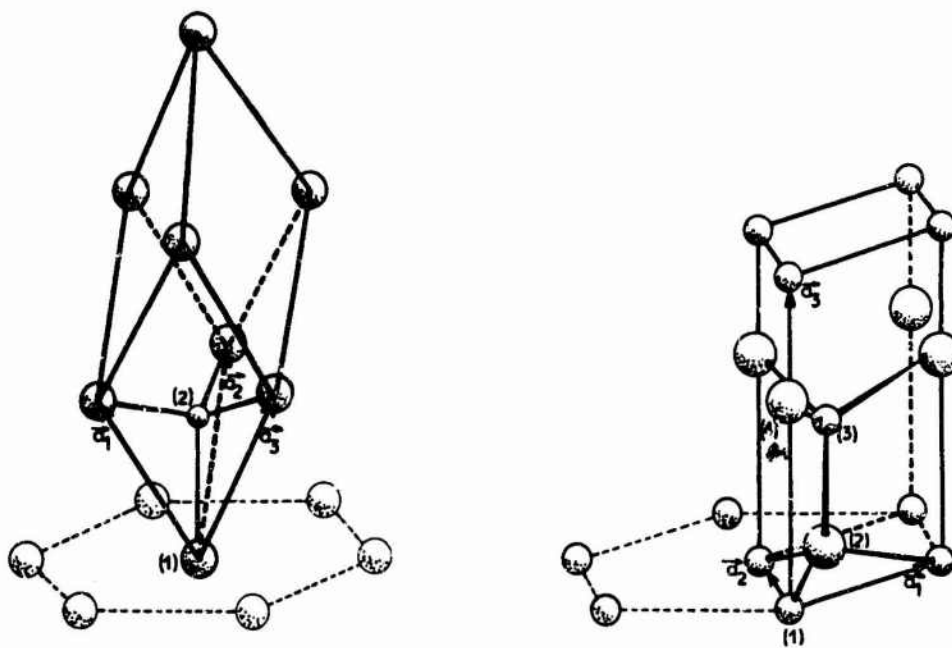
Figure 2. Representation of elementary cells :
a) left   cubic structure
b) right hexagonal structure

The first nearest neighbours in both structures are at the corners of a regular tetrahedron related to those of the group IV semiconductors. For this reason many physical properties are analogous in both types of crystal lattices.

The two respective environments in the cubic and hexagonal structure are shown in Fig.3.
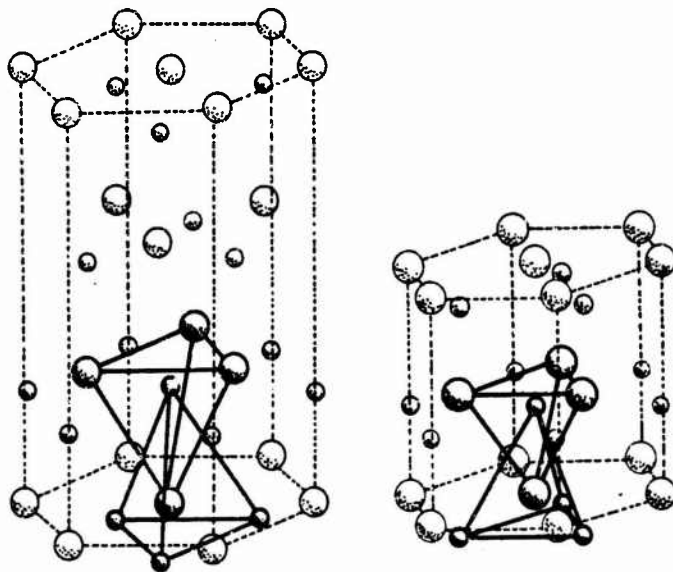
Figure 3.   Environments in the cubic left and hexagonal right structure.

The bounding in the crystals of the II-VI compounds spares the complete gap from ionic to covalent.

The first Brillouin zone deduced from this structure is shown in Fig.4 respectively for the blende and the wurtzite.
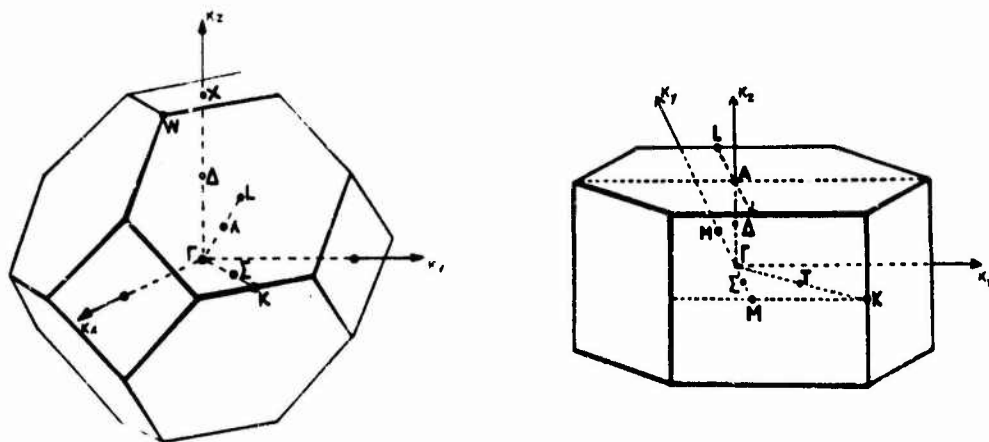
Figure 4. First Brillouin zone for Blende and Wurtzite.

3. Dispersion Relations.

In the harmonic approximation where the potential energy of a crystal is expanded in power of the displacement of the atoms from their equilibrium positions and the expansion is broken off the quadratic terms, the equation of motion of the atom k with mass m_k in the unit cell l subject to the displacement u_α with $\alpha = x, y, z$ is given by

$$m_k \ddot{u}_\alpha\binom{l}{k} + \sum_{l'k'} \sum_\beta \Phi_{\alpha\beta}\binom{ll'}{kk'} u_\beta\binom{l'}{k'} = 0 \qquad (3.1)$$

where Φ is the force constant matrix depending only on the distance between cells $\underline{r}(l)-\underline{r}(l')$ due to the periodic symmetry of the lattice.

The normal modes and their frequencies are solutions of the set of equations for all unit cells of the crystal. Because of the periodic symmetry the modes have wave like phase variation from cell to cell and specific relative motion in the cell.

The dynamical matrix being of the form

$$C_{\alpha\beta}\binom{q}{k\ k'} = \sum_l \frac{\Phi_{\alpha\beta}\binom{l}{k\ k'}}{(m_k m_{k'})^{1/2}} \ \exp[-i\underline{q}.\underline{r}(l)] \qquad (3.2)$$

the system of $3n$ linear and homogenious equations has non-vanishing solutions only if the determinant

$$C_{\alpha\beta}\binom{q}{k\ k'} - \omega^2 \delta_{kk'} \ \delta_{\alpha\beta} = 0 \qquad (3.3)$$

vanishes.

This "characteristic" equation gives the chracteristic frequencies $\omega(\underline{q})$ whose graphic representations are the dispersion curves of the crystal.

A certain number of investigations have been developed aiming the knowledge of the dispersion curves of the II-VI compounds. Some of them [1,2] based on the shell model develop the formal discussion without actually doing the calculations. Calculating the dispersion relations of blends or wurtzite structures in the shell model would involve a large number of parameters which make such calculations meaningless.

Merten [3] has developed a series of studies in which the lattice vibrations of blends and wurtzite structures are investigated on microscopic basis considering the dynamical matrix without and with long range Coulomb interactions. Here again the numerical calculations have not been carried out throughout the whole Brillouin zone and only the optical modes at the center of the Brillouin zone have been deduced.

Recently Nusimovici and Birman [4] have performed the explicite calculations of the dispersion relations for CdS-wurtzite structur.. The single phonon frequencies have been used to calculate the force constants. The model considers short range interactions corresponding to central forces between first, second and third neighbours and to central angular forces between first and second neighbours, as well as long range Coulomb interactions depending on a parameter having the dimensions of a spring constant.

The wurtzite is supposed to be ideal and from the point of view of the short range interactions the anisotropy is represented by the third neighbour forces as shown on Fig.5.
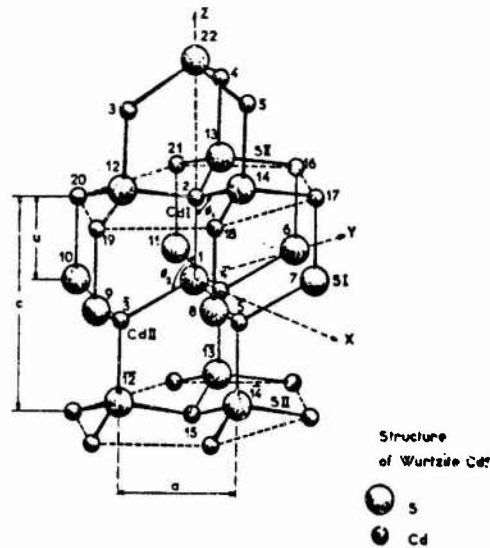
Figure 5. Anisotropy deduced from short range interaction in Wurtzite.

The short range potential is written as

$$V^{SR} = \frac{1}{2} \sum_{1^\circ} \lambda(\delta r_{ij})^2 + \frac{1}{2} \sum_{2^\circ Cd} \mu(\delta r_{jl})^2 + \frac{1}{2} \sum_{2^\circ S} \nu(\delta r_{ik})^2$$

$$+ \frac{1}{2} \sum_{3^\circ} \delta(\delta r_{il})^2 + \frac{1}{2} \sum_{S-Cd-S} k_\theta r_o^2 (\delta\theta_{ijk})^2$$

$$+ \frac{1}{2} \sum_{Cd-S-Cd} k_{\theta'} r_o^2 (\delta\theta_{jkl})^2 + \frac{1}{2} \sum_{Cd-S-Cd} k_{r\theta'} r_o^2 (\delta\theta_{jkl})(\delta r_{jk})$$

$$+ \frac{1}{2} \sum_{S-Cd-S} k_{r\theta} r_o^2 (\delta\theta_{ijk})(\delta r_{ij})$$

where λ, μ, ν, and δ, correspond to central forces between first, second and third neighbours, k_θ, $k_{\theta'}$, $k_{r\theta}$ and $k_{r\theta'}$ correspond to non-central angular forces between first and second neighbours.

The Coulomb part has been determined by summing the second derivatives of

$$V^C = \sum_{\substack{lk \\ l'k'}} \frac{e_k \, e_{k'}}{|\, r(l,k) - r(l,k')|}$$

using the Ewald transformation.

The Coulomb field is proportional to a parameter $\rho = q^2/a^3$ having the dimensions of a spring constant, q being the effective charge of the ion and a is a lattice parameter. The values of the parameters taken in this first calculations are the following :

$$\lambda = 1.061 \times 10^5 \text{ dyn/cm} ,$$
$$\mu = 0.203 \times 10^5 \text{ dyn/cm} ,$$
$$\nu = -0.086 \times 10^5 \text{ dyn/cm} ,$$
$$\delta = -0.085 \times 10^5 \text{ dyn/cm} ,$$
$$k_\theta = 0.170 \times 10^5 \text{ dyn/cm} ,$$
$$k_{\theta'} = 0.154 \times 10^5 \text{ dyn/cm} ,$$
$$K_{r\theta} = k_{r\theta} + k_{r\theta'} = -0.0216 \times 10^5 \text{ dyn/cm} ,$$
$$\rho = 0.032 \times 10^5 \text{ dyn/cm} .$$

The dispersion curves of wurtzite for the ΓA, ΓM and ΓK directions of the Brillouin zone calculated by this method are given in Fig.6.

Figure 6. Dispersion curves of Wurtzite for the M, Γ, A and K points of the Brillouin Zone.

A calculation done for an hypothetical cubic CdS shows the differences between the two phases : wurtzite and blende.
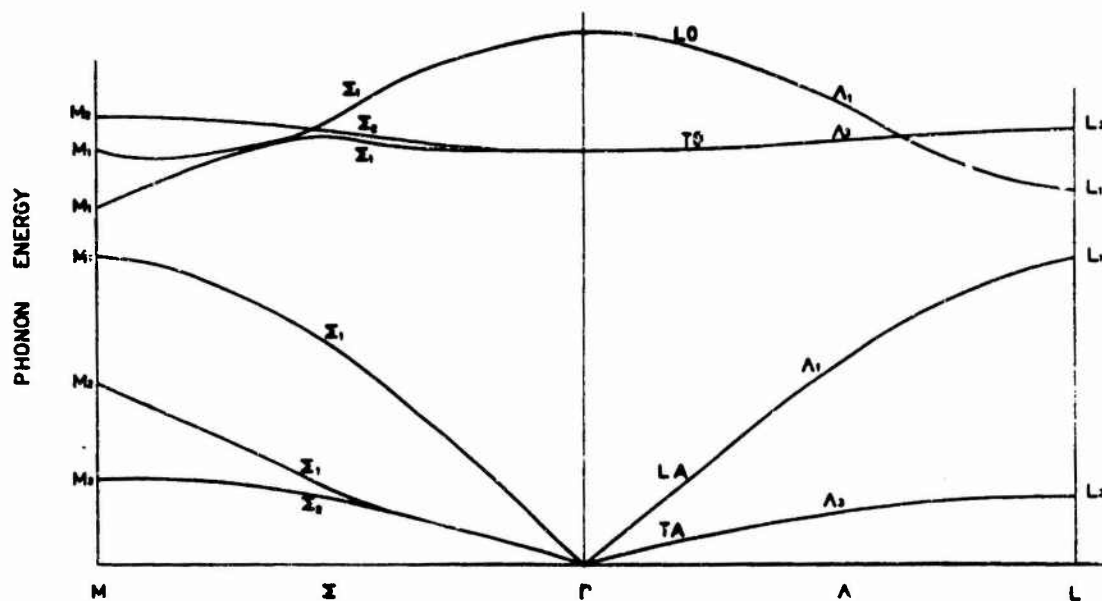
<u>Figure 7</u>.   Dispersion relations for Blende for the M, Γ and L points
of the Brillouin Zone.

An important check of their calculation is given by the two-phonon optical data obtained by infrared and Raman spectra. Table I compares the two-phonon Raman scattering in CdS calculated by Nusimovici and Birman with the ones obtained by Tell, Damen and Porto [5].

In more recent work [6] Nusimovici and Birman made a direct comparison between infrared spectra obtained experimentally [7] and the calculated two-phonon density of modes.

Table I

Two-phonon Raman scattering in CdS-wurtzite

Experiment (cm^{-1})	Interpretation	Calculation (cm^{-1})
97	$2\Gamma_6$	90
	$2M_4$	86
207	$M_1 \oplus M_3$	201
	$M_2 \oplus M_3$	202
	$K_2 \oplus K_3$	209
	$K_3 \oplus K_3$	210
328	$M_2 \oplus M_4$	323
	$M_3 \oplus M_4$	328
	$K_1 \oplus K_3$	331
347	$A_1 \oplus A_3$	342
	$M_1 \oplus M_2$	345
	$M_1 \oplus M_1$	344
	$M_2 \oplus M_2$	346
	$M_1 \oplus M_3$	342
	$M_3 \oplus M_3$	346
	$K_2 \oplus K_3$	347
	$K_2 \oplus K_2$	346
	$K_3 \oplus K_3$	344
	$K_3 \oplus K_2$	346
364	$A_1 \oplus A_1$	363
	$K_1 \oplus K_2$	368
	$K_1 \oplus K_3$	369
	$M_1 \oplus M_1$	368
556	$2K_1$	558
	$2M_3$	550
605	$2\Gamma_1$	596
	$2\Gamma_5(L)$	616

4. Photon-Phonon Interaction.

One of the main possibility to obtain experimental precisione on the diepereion relations and particularly the normal modee frequenciee at the center and the edgee of the Brillouin zone are infrared spectroscopy and Raman scattering. For the II-VI compounde of blende and wurtzite etructures theee two methode are complementary becauee of particular eelection rulee based on eymmetry coneiderations.

The optical absorption is given by the transition probability proportional to a matrix element which is different from zero only when energy and momentum conservation rules are obeyed. The matrix element for optical absorption depends on the dipole moment operator $\underline{V}$. It is then easy to deduce by group theory arguments the optically active normal modes in blende and wurtzite structures. These are often different from that active in Raman scattering while in those cases the matrix element is related to the polarizability tensor π.

4.1. Infrared Dispersion.

When the electromagnetic field acts on the crystal there is a coupling between the elastic waves giving the phonon fields and the electromagnetic waves giving the photon fields.

The electromagnetic field is given by Maxwell's equations :

$$\text{rot } H = \frac{1}{c}\dot{D} \; ,$$

$$\text{rot } E_{int} = -\frac{1}{c}\dot{H} \; ,$$

$$\text{div } D = 0 \; , \tag{4.1}$$

$$\text{div } H = 0 \; ,$$

$$\text{and } D = E_{int} + 4\pi p \; . \tag{4.2}$$

The phonon field is described by the induced polarization due to the displacement in opposite directions of the two sublattices formed by charged ions and the internal electric field E_{int} equal to the macroscopic electric field in the crystal,

$$p = N\, e_T\, u + \frac{\varepsilon_\infty - 1}{4\pi}\, E_{int} \; , \tag{4.3}$$

and also by the equation of motion

$$M\ddot{u} + \left(M\omega_o^2 - \frac{4\pi N\, e_s\, e_T}{3}\right)u = e_T\, E_{int} \; . \tag{4.4}$$

The solutions of the coupled system of equations representing the radiation field and the phonon field give the infrared dispersion for a given crystal.

A detailed analysis of infrared dispersion for blende and wurtzite structures has been carried out by Le Toullec [8] ; this chapiter summarize the results.

4.1.1. Blende.

In a rigid ion approximation when the ionic charge is centered on the ion, the dynamical matrix can be written in two terms :

$$C_{\alpha\beta}\begin{pmatrix} q \\ k \ k' \end{pmatrix} = C^N_{\alpha\beta}\begin{pmatrix} q \\ k \ k' \end{pmatrix} + C^C_{\alpha\beta}\begin{pmatrix} q \\ k \ k' \end{pmatrix} \quad . \tag{4.5}$$

The first term concerns the short range interaction and the second the Coulomb interaction due to long range forces. The polar modes which are infrared active arise from these Coulomb forces.

The first term gives all the normal modes. For $q = 0$ the secular equation $(C - \omega^2 I)$ gives two distinct roots threefold degenerate :

$$\omega_{ac} = 0 \quad ,$$

$$\omega_{op} = \left[\frac{m_1 + m_2}{m_1 \ m_2} \sum_1 N_{xx}\begin{pmatrix} 1 \\ 1 \ 2 \end{pmatrix} \right]^{1/2} \quad . \tag{4.6}$$

The displacement vectors corresponding to ω_{ac} are $u_1 = u_2$, with the two sublattices moving in the same direction, those corresponding to ω_{op} are $u_1 = -(m_2/m_1)u_2$, with the two sublattices moving in opposite directions. To the optical modes corresponds on induced dipole moment equal to

$$M = e^* u_1 \frac{m_1 + m_2}{m_2} \quad . \tag{4.7}$$

In a rigid non-polarizable ions approximation the Coulomb potential energy can be written

$$\Phi = \frac{1}{2} \sum_{\substack{ll' \\ kk'}} \frac{e_k \ e_{k'}}{r\begin{pmatrix} l \\ k \end{pmatrix} - r\begin{pmatrix} l' \\ k' \end{pmatrix}} \tag{4.8}$$

and the coefficients C^C deduced from Φ for $q = 0$ are

$$C^C_{\alpha\beta}\begin{pmatrix} 0 \\ k \ k' \end{pmatrix} = - \frac{4\pi \ N \ e_k \ e_{k'}}{(m_k m_{k'})^{1/2}} \left(\frac{\delta_{\alpha\beta}}{3} - \frac{q_\alpha q_\beta}{q^2} \right) \tag{4.9}$$

where N is the number of ion paires per unit volume. If we have the propagation vector q along the Oz axes we obtain now two optical branches instead of one. The first ω_{TO} is twofold degenerate corresponding to vibrations perpendicular to q :

$$\omega_{TO}^2 = \omega_0^2 - \frac{4\pi \ N \ e_1^2}{3M} \qquad \text{where} \quad M = \frac{1}{m_1} + \frac{1}{m_2} \tag{4.10}$$

where ω_0 is the optical frequency when the Coulomb forces are neglected and the second ω_{LO} non-degenerate corresponding to vibrations parallel to q :

$$\omega_{LO}^2 = \omega_0^2 + \frac{8\pi\,N\,e_1^2}{3M} = \omega_{TO}^2 + \frac{4\pi\,N\,e_1^2}{M} \quad . \tag{4.11}$$

Compared to equation (4.4) we see that these two equations differ by the effective charge e_1^2 instead of $e_s e_T$ due to the fact that we have considered rigid non-polarizable ions.

The displacement in the case of polarizable atoms will be

$$u = \frac{e_T\,E_{int}}{M(\omega_{TO}^2 - \omega^2)} \quad . \tag{4.12}$$

Substituting in equation (4.3) and subsequently in equation (4.2) we obtain the equation of optical dispersion of the crystal

$$\varepsilon(\omega) = \varepsilon_\infty + \frac{4\pi\,N\,e_T^2}{M(\omega_{TO}^2 - \omega^2)} \tag{4.13}$$

and in the limit $\omega = 0$ we have the static dielectric constant

$$\varepsilon_0 = \varepsilon_\infty + \frac{4\pi\,N\,e_T^2}{M\,\omega_{TO}^2} \tag{4.14}$$

where from

$$\varepsilon(\omega) = \varepsilon_\infty + \frac{(\varepsilon_0 - \varepsilon_\infty)\,\omega_{TO}^2}{\omega_{TO}^2 - \omega^2} \tag{4.15}$$

two cases can be distinguished.

First case : $\varepsilon = 0$; $u \parallel q \parallel E_{int}$: longitudinal wave.

$$\varepsilon = 0 = \varepsilon_\infty + \frac{(\varepsilon_0 - \varepsilon_\infty)\omega_{TO}^2}{\omega_{TO}^2 - \omega^2} \tag{4.16}$$

hence

$$\omega_L^2 = \omega_{TO}^2\,(\varepsilon_0/\varepsilon_\infty) = \omega_{TO}^2 + \frac{4\pi\,N\,e_T^2}{M\,\varepsilon_\infty} \quad . \tag{4.17}$$

This frequency is independent of the wave vector q and is equal to the longitudinal optical frequency of the system without the external field being applied.

Second case : $u \perp q \perp E_{int}$: transverse wave.

From Maxwell's equations one deduces

$$\frac{c^2 q^2}{\omega^2} = \varepsilon_\infty + \frac{(\varepsilon_0 - \varepsilon_\infty)\omega_{TO}^2}{\omega_{TO}^2 - \omega^2} = \varepsilon(\omega) \quad . \tag{4.18}$$

The incident light interacts strongly with transverse optical phonons of the crystal. The normal mode of the coupled system : photon + phonons (TO) is called polariton. The dispersion relation of polaritons describes the phenomena of optical dispersion. The dispersion $\omega = f(q)$ curve could be easily deduced if one considers the Lyddane-Sachs-Teller relation

$$\omega_{LO}^2 = \omega_{TO}^2 \, (\varepsilon_o / \varepsilon_\infty) \quad . \tag{4.19}$$

Equation (4.18) is now written

$$q^2 = \frac{1}{c^2} \, \varepsilon_\infty \, \omega^2 \, \frac{\omega^2 - \omega_{LO}^2}{\omega^2 - \omega_{TO}^2} \quad . \tag{4.20}$$

The dispersion curve of polariton gives $\omega = f(q)$ for a system of coupled photons plus optical phonons is represented in Fig.8.
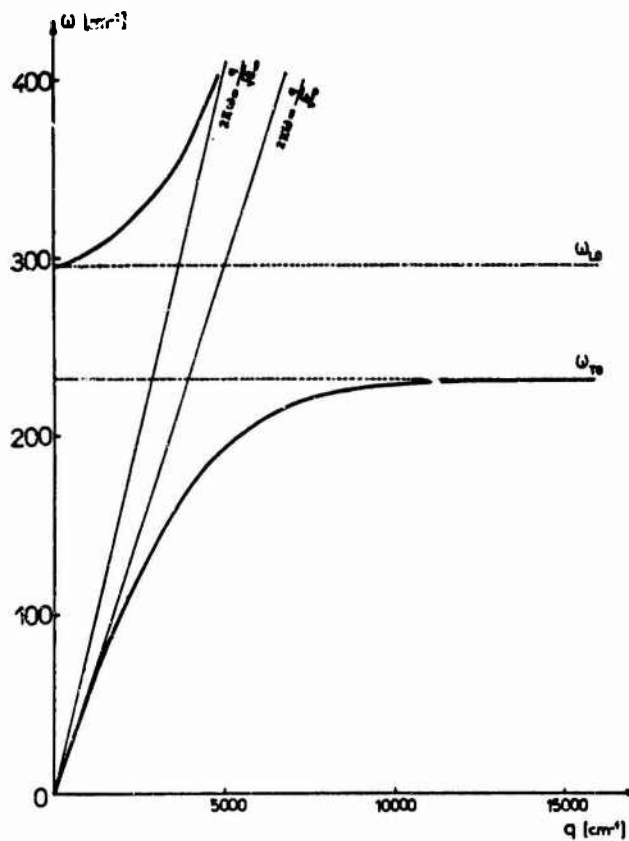
Figure 8. Dispersion curve of optical phonons coupled with photons.

4.1.1.a) Introduction of Damping.

In the harmonic approximation all phonons are independent from each other and therefore the equations of motion are linear. In reality the system of equations is coupled through the unharmonic terms of the potential. Part of the electromagnetic energy brought into the TO by the incident radiation field is transferred to other phonons. The introduction of a damping constant in the phenomenological equations expresses this fact and the equation of motion becomes

$$m \ddot{u} + m \gamma \dot{u} + m \omega_{TO}^2 u = e_T E_{int} \quad . \tag{4.21}$$

Equation (4.15) should now be written

$$\varepsilon(\omega) = \varepsilon_\infty + \frac{(\varepsilon_0 - \varepsilon_\infty)\omega_{TO}^2}{\omega_{TO}^2 - \omega^2 - i\gamma\omega} = (n + ik)^2 \quad . \tag{4.22}$$

The real and imaginary parts of the dielectric constant are then :

$$\varepsilon_r = n^2 - k^2 = \varepsilon_\infty + \frac{(\varepsilon_0 - \varepsilon_\infty)(\omega_{TO}^2 - \omega^2)\omega_{TO}^2}{(\omega_{TO}^2 - \omega^2)^2 + \gamma^2 \omega^2} \quad , \tag{4.23}$$

$$\varepsilon_i = 2nk = \frac{(\varepsilon_0 - \varepsilon_\infty)\omega_{TO}^2 \gamma\omega}{(\omega_{TO}^2 - \omega^2) + \gamma^2 \omega^2} \quad . \tag{4.24}$$

The frequency ω_T, pole of $\varepsilon(\omega)$, can be written

$$\omega_T = \omega_r + i\omega_i \tag{4.25}$$

with

$$\omega_r = [\omega_{TO}^2 - (\gamma^2/4)]^{1/2} = \omega_{TO}[1 - (\gamma/2\omega_{TO})^2]^{1/2}$$

and

$$\omega_i = -\frac{\gamma}{2} \quad . \tag{4.26}$$

The real part of ω_T represents the resonance frequency and differs very little from ω_{TO} since $(\gamma/\omega_{TO}) \ll 1$
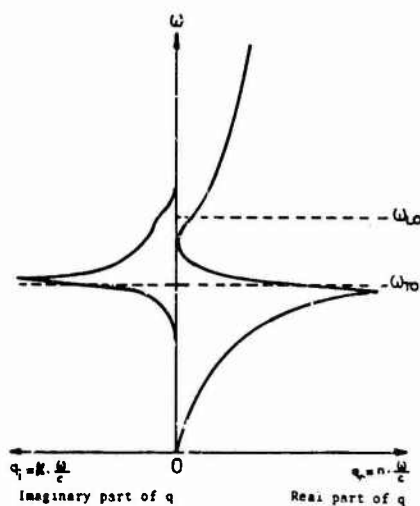
The imaginary part of ω_1 measures the damping.

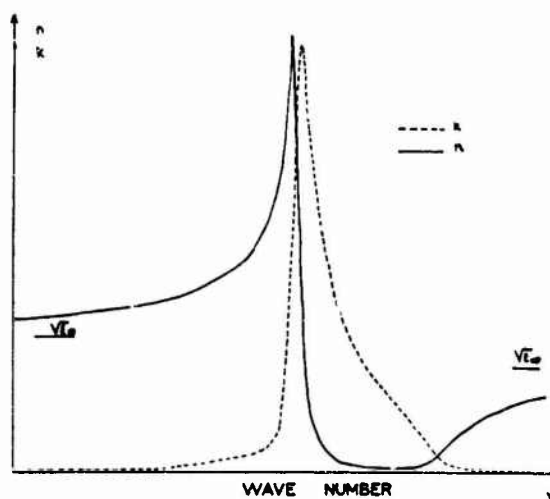ω_L is a root of $\varepsilon(\omega) = 0$ and can be written

$$\omega_L = [\omega_{LO}^2 - (\gamma^2/4)]^{1/2} - [i\gamma/2] \quad . \tag{4.27}$$
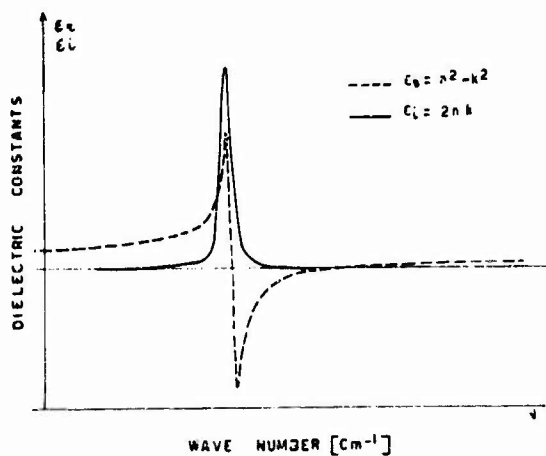
The infrared dispersion curves for the transverse modes are represented on Fig.9.

Figure 9. Anharmonic dispersion curve for the TO mode.

Figure 10. Anharmonic optic constants.

Figure 11. Anharmonic dielectric constants.

4.1.1.b) <u>Experimental results from infrared spectro-
scopy</u>.

Dispersion in blende type crystals has been studied by many
authors. In recent years systematical studies have been developed
as well by reflectivity as by absorption measurements in the infra-
red region. Recent results for blende are summarized on Table II.

<u>Table II</u> - Blende

Frequencies of the optically active modes in
Blende type crystals determined by infrared
spectroscopy.

	ω_{TO}	ω_{LO}	ε_0	ε_∞	References
ZnS	274	350	8.3	5,07	a, b
ZnSe	207	242	7,6	5.4	c
	209.5	250	8.1	5.75	d
	209	257	9.2	6.1	e
			9.1		f
			8.66		g
				5.90	h
ZnTe	177	205	9.1	6.7	c
			10.1		f
			9.67		g
				7.28	h
CdTe	141	168	10.2	7.13	c
			9.6		f
			9.65		g
				7.21	h

a) Le Toullec, Thesis, Paris.

b) C.Hass and J.P.Mathieu, J. Phys. Radium <u>15</u>, 492 (1954).

c) A.Mitsuishi, Paper presented at "U.S.-Japan Cooperative Seminar
on far infrared spectroscopy", Colombus, Ohio, Sept.1965.

d) M.Aven, D.T.F.Marple and B.Segall, J. Appl. Phys. <u>32</u> Suppl.,
2261 (1961).

e) S.S.Mitra, J. Phys. Soc. Japan <u>21</u> Suppl., 61 (1966).

f) D.Berlincourt, H.Jaffe, L.R.Shiozawa, Phys. Rev. <u>129</u>, 1009 (1963).

g) S.Roberts and D.T.F.Marple (1967), To be published.

h) D.T.F.Marple, J. Appl. Phys. <u>35</u>, 539 (1964).

4.1.2. Wurtzite.

4.1.2.a) Short range forces.

The unit cell contains 4 atoms 2 anions and 2 cations, 12 branches are therefore expected in the dispersion curves.

The following relation between C coefficients results from the crystal symmetry :

$$C_{xx}^{N}\binom{0}{k\ k'} = C_{yy}^{N}\binom{0}{k\ k'} \neq C_{zz}^{N}\binom{0}{k\ k'} \ . \tag{4.28}$$

One obtains 6 different solutions of the secular equation. One is threefold degenerated and corresponds to the acoustical branches. From the 5 other solutions for the optical frequencies 2 are non-degenerate, 2 are twofold degenerate and one threefold degenerate due to an accidental degeneracy for $\omega_{1\perp} = \omega_{1//}$.

The relative motion of the four atoms constituting the unit cell is schematically represented on Fig.12.
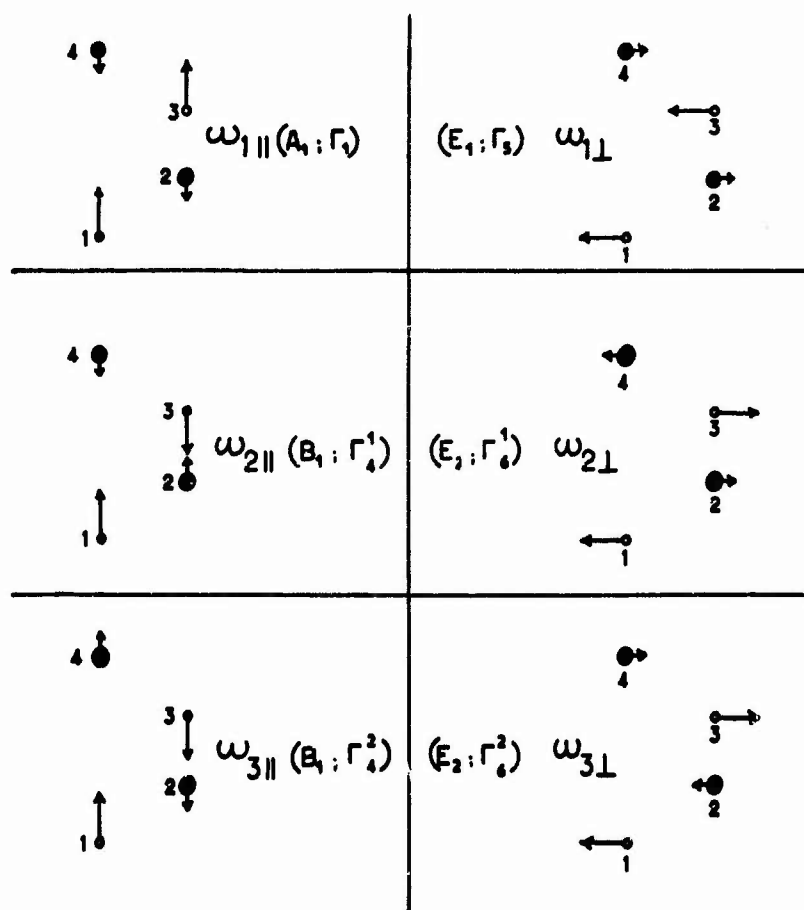
Figure 12. Relative motion of the four atoms in the hexagonal unit cell.

In the optical modes of vibration for the frequency ω_1 the sub-lattices with the same kind of atoms (1) and (3) are moving in the same direction and the sublattices with atoms (2) and (4) in opposite directions. The displacement vectors are related by

$$\underset{\sim}{u}_\alpha(1) = - \frac{m_2}{m_1} \underset{\sim}{u}_\alpha(2) = \underset{\sim}{u}_\alpha(3) = - \frac{m_2}{m_1} \underset{\sim}{u}_\alpha(4) \quad . \qquad (4.29)$$

This kind of displacement results into a total dipole moment per unit cell :

$$M = 2 e^* \underset{\sim}{u}_1 \frac{m_1 + m_2}{m_2} \qquad . \qquad (4.30)$$

For the modes of frequencies ω_2 and ω_3 the displacement vectors are of the same type but the induced dipole moment per unit cell is always equal to zero and therefore these modes are not optically active.

Fig.13 shows the relative position of the normal mode frequencies near the center of the Brillouin zone deduced only from the consideration of the nearest neighbours short range interaction.
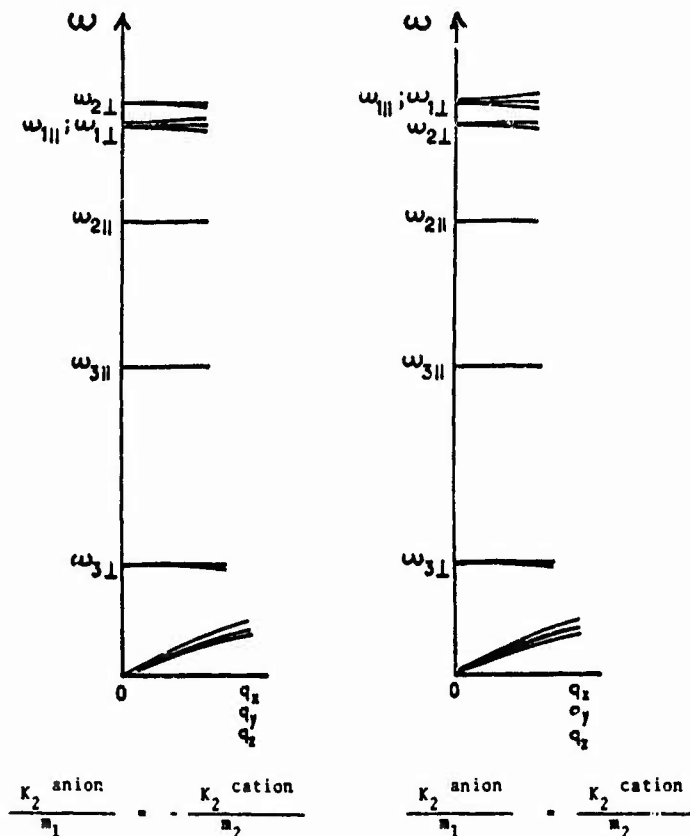
Figure 13.   Position of the normal mode frequencies near q = 0 in the case of short range interaction only.

4.1.2.b) Long range Coulomb forces.

The coefficient C^C deduced from the Coulomb potential energy can be written in the case of wurtzite :

$$C^C_{\alpha\beta}\binom{0}{k\ k'} = - \frac{N\ e_k\ e_{k'}}{(m_k m_{k'})^{1/2}} (L^{kk'}_\alpha\ \delta_{\alpha\beta} - \frac{4\pi\ q_\alpha\ q_\beta}{q^2})\ ,\ (4.31)$$

$L^{kk'}_\alpha$ are Lorentz factors in anisotropic crystals and their numerical values are known.

Introducing Coulomb interaction into the determination of the normal mode frequencies one have also to distinguish between the case where the propagation vector q is parallel or perpendicular to the optical axis c. The modes corresponding to atom vibrations perpendicular to the propagation vector labelled TO and these to parallel vibration LO, $//$ and $\perp$ refers to the vibration of the atoms with regard to the c axis. The optically active triply degenerate mode ω_1 without Coulomb interaction, splits now into the following frequencies :

For $q \perp c$:

$$\omega^2_{LO} = \omega_{1\perp} + 8.47\ \frac{Ne^2}{M}\ ;\ \omega_{TO\perp} = \omega_{1\perp} - 4.09\ \frac{Ne^2}{M}\ ;\ \omega_{TO//} = \omega^2_{1//} - 4.39\ \frac{Ne^2}{M}\ .$$

For $q // c$:

$$\omega_{LO//} = \omega_{1//} + 8.17\ \frac{Ne^2}{M}\ ;\ \ \omega_{TO\perp} = \omega_{1\perp} - 4.09\ \frac{Ne^2}{M}\ .$$

Here N is the number of unit cell per cm^3, e is the electronic charge, and M the reduced mass : $M = m_1 m_2/(m_1 + m_2)$. These results are schematically represented in Fig.14.

4.1.2.c) Infrared dispersion curves.

Wurtzite being on uniaxial crystal, because of the anisotropy, the infrared dispersion curves depend on the direction of propagation. The solutions of the coupled equations giving the radiation field and the phonon field are now of the form :

$$(n^2 - \epsilon_\perp)\ [(n^2 - \epsilon_\perp)(n^2 - \epsilon_{//}) - n^2 \sin^2\theta(n^2 - \epsilon_{//}) - n^2 \cos^2\theta(n^2 - \epsilon_\perp)]\ = 0\ .\ (4.32)$$

θ is the angle between the propagation vector and the optical axis. Two types of solutions represented in Fig.15 appears.

20
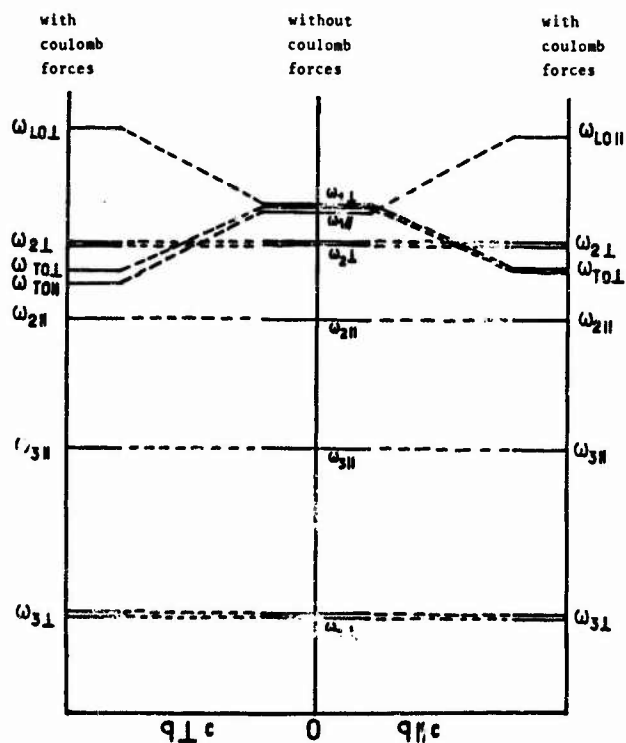
Figure 14. Splitting of dispersion curves near q = 0 when Coulomb forces are taking into account.

a) on the left the propagation vector is perpendicular to the c axis

b) on the right the propagation vector is parallel to the c axis.
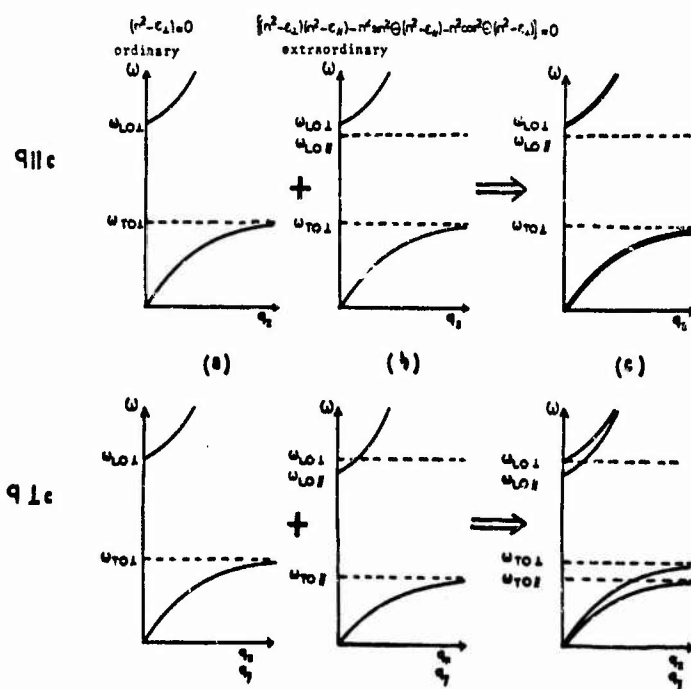
Figure 15. Dispersion curve dependance on the direction of propagation

a) $q \parallel c$

b) $q \perp c$

A) Ordinary solution.

$$n^2 - \varepsilon_\perp = 0 \ .$$

This solution is independent of the angle θ (Fig.4a). The corresponding dispersion relation is

$$q^2 = \frac{1}{c^2} \, \varepsilon_{\infty\perp} \, \omega^2 \, \frac{\omega^2 - \omega_{LO\perp}^2}{\omega^2 - \omega_{TO\perp}^2} \ . \tag{4.34}$$

B) Extraordinary solution.

This second solution corresponding to the second factor of the equation (4.32) depending on the angle θ. Two extreme cases can be considered :

$\theta = 0$ i.e. $q \mathbin{/\!/} c$ and $\theta = \frac{\pi}{2}$ i.e. $q \perp c$

- First case : $q \mathbin{/\!/} c$; $\theta = 0$.

The equation (4.32) becomes now :

$$\varepsilon_{/\!/}(n^2 - \varepsilon_\perp) = 0 \quad . \tag{4.35}$$

$\varepsilon_{/\!/} = 0$ gives $\omega = \omega_{LO/\!/}$, solution independent of q.

The infrared active longitudinal phonon $\omega_{LO/\!/}$ do not influence the infrared dispersion in the considered direction.

$n^2 - \varepsilon_\perp = 0$ gives the second transverse solution (Fig.4b) with the same dispersion relation as equation (4.34).

- Second case : $q \perp c$; $\theta = \frac{\pi}{2}$.

Equation (4.32) becomes

$$\varepsilon_\perp(n^2 - \varepsilon_{/\!/}) = 0 \tag{4.36}$$

where $\varepsilon_\perp = 0$ with $\omega = \omega_{LO\perp}$.

$n^2 - \varepsilon_{/\!/} = 0$ with the dispersion solution :

$$q^2 = \frac{1}{c^2} \, \varepsilon_{\infty/\!/} \, \omega^2 \, \frac{\omega^2 - \omega_{LO/\!/}^2}{\omega^2 - \omega_{TO/\!/}^2} \ . \tag{4.37} \ (\text{Fig.4b})$$

We have seen that $\omega_{TO\perp}$ is a transverse optical mode $u \perp q$ with $u \perp c$; $\omega_{TO/\!/}$ is a transverse optical mode $u \perp q$ with $u \mathbin{/\!\!/} c$. The solutions of equation (4.32) are given on the Fig.4c.

Experimental determination of these frequencies are made by the following two methods.

1) <u>Single crystals of large dimensions.</u>

The reflectivity is measured under weak incidence angle ($\theta \sim 15°$). The curves representing the refractive index $n(\omega)$ and the extension coefficient $K(\omega)$ are calculated by means of Kramers-Krönig inversion formula.

The ω_{TO} frequency is the frequency for which the quantity ($2nK\omega$) has its maximum.

The ω_{LO} frequency is the frequency for which one has the relation $n^2-K^2 = 0$ with $(\partial n/\partial \omega) > 0$.

In order to be able to determine the four frequencies $\omega_{TO//}$, $\omega_{TO\perp}$, $\omega_{LO//}$, $\omega_{LO\perp}$, it is sufficient to prepare a sample with c axis perpendicular to the plane of incidence and to use a polarized light beam either parallel to the c axis in which case one obtains $\omega_{LO//}$ and $\omega_{TO//}$, or perpendicular to the c axis in which case one obtains $\omega_{LO\perp}$ and $\omega_{TO\perp}$.

2) <u>Thin films.</u>

When transmission or reflectivity measurements are performed on thin films under oblic incidence and with a light beam polarized in the plane of incidence, the transverse optical as well as the longitudinal optical modes interact with the infrared radiation and hence their frequencies can be measured directly. In the case of an uniaxial crystal if the thin film is such as to have the c axis perpendicular to the substrate one measures then $\omega_{LO//}$ and the $\omega_{TO\perp}$ frequencies. This is the case of CdS thin films evaporated on silicon single crystal substrates.

If the c axis is parallel to the surface of the layer it is then possible to observe $\omega_{LO\perp}$.

The different experimental situations in which measurements have been made by Le Toullec [8] are listed in Fig.16.
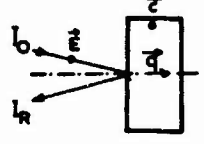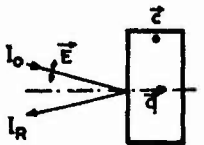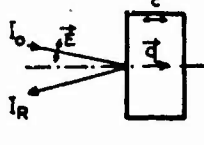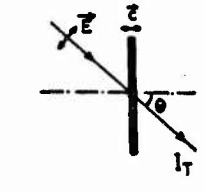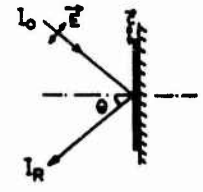
(16) thick crystals	active modes	frequencies calculated by Kramers Krönig inversion
$\vec{E} \parallel \vec{c}$ $\vec{q} \perp \vec{c}$	LO $\perp$ TO $\parallel$	$\omega_{LO\parallel}$ $\omega_{TO\parallel}$ fig. $\begin{pmatrix} 6. b \\ q \perp c \end{pmatrix}$
$\vec{E} \perp \vec{c}$ $\vec{q} \perp \vec{c}$	LO $\perp$ TO $\perp$	$\omega_{LO\perp}$ $\omega_{TO\perp}$ fig. $\begin{pmatrix} 6. a \\ q \perp c \end{pmatrix}$
$\vec{E} \perp \vec{c}$ $\vec{q} \parallel \vec{c}$	LO $\parallel$ TO $\perp$	$\omega_{LO\perp}$ $\omega_{TO\perp}$ fig. $\begin{pmatrix} 6a,b \\ q \parallel c \end{pmatrix}$

thin crystals	active modes	observed frequencies
E sin θ $\parallel$ c E cos θ $\perp$ c $\vec{q} \parallel \vec{c}$	LO $\parallel$ TO $\perp$	$\omega_{LO\parallel}$ $\omega_{TO\perp}$
E sin θ $\perp$ c E cos θ $\parallel$ c $\vec{q} \perp \vec{c}$	LO $\perp$ TO	$\omega_{LO\perp}$ $\omega_{TO\parallel} < \omega_{TO} < \omega_{TO\perp}$

Figure 16.   Comparison of the optical frequencies of bulk samples and thin films, under oblique incidence and with polarized light.

The experimental results are summarized in Table III.

Table III - Wurtzite.

Frequency of the optically active modes in
wurtzite structure crystals determined by
infrared spectroscopy.

	$\omega_{TO}//$ cm⁻¹	$\omega_{TO}\perp$ cm⁻¹	$\omega_{LO}//$ cm⁻¹	$\omega_{LO}\perp$ cm⁻¹	$\varepsilon_{c}//$	$\varepsilon_{c}\perp$	$\varepsilon_{\infty}//$	$\varepsilon_{\infty}\perp$	References
	232	240	298	302	8.9	8.40	5.38	5.3	a
	233.6	241.2	299	305	8.9	8.50	5.38	5.29	b
CdS					9.53	9.02			c
	235	242	296	303	8.42	8.37	5.32	5.32	d
	167	171	209	211.5	9.95	9.1	6.05	5.95	a
	166	172	211	210	10.16	9.29	6.3	6.2	e
CdSe							6.05	5.95	f
					10.20	9.53			c
	168	171	211	211	9.6	9.3	6.1	6.1	d

References

a) Le Toullec, Thesis, Paris.

b) A. Mitsuishi, Paper presented at "U.S.-Japan Cooperative Seminar on far infrared epectroecopy", Colombus, Ohio, Sept. 1965.

c) D. Berlinccurt, H. Jaffe, L.R. Shiozawa, Phye. Rev. 129, 1099 (1963).

d) H.W. Verleur and A.S. Barker Jr., Phys. Rev. 155, 750 (1967).

e) S.S. Mitra, J. Phys. Soc. Japan 21 Suppl., 61 (1966).

f) Shiozawa and al., Research on II-VI compound semiconductore, 6th quarterly Report, Contract No AF 33 (657) - 7399 U.S. Air Force Aeronautical Reeearch Laboratories, Wright-Patterecn Air Force Base, Ohio.

4.2. Light scattering.

The inelastic ecattering of the phonons by the crystal is generally referred to ae Raman ecattering if optical phonone are involved in the processus and as Brillouin scattering if the acoustical branches are involved. Phonone may be absorbed or emitted and accordingly stokes or antistokee linee will be observed on the long wave eide or the short wave side of the incident radiation. The polarieibility of the cryetal ie composed of two parte : one due to the nuclear displacements and the other to the consequent electronic polarization.

In first order the diffused intensity for the stokes Raman line in the harmonic approximation is

$$I_{stokes} = K \, \nu_{diff}^4 \, [\frac{n_p+1}{\nu_0}] \, [e_a^i \, \alpha_{ab}' \, e_b^{diff}]^2 \quad ,$$

n_p is the number of phonons occupying the initial p state, ν_0 is the oscillator's frequency, e_a^i is the ath component of the unit polarization vector of the incident radiation, e_b^{diff} is the bth component of the polarization unit vector of the diffused light, $\alpha_{ab}'(q_e) = \partial\alpha_{ab}/\partial q_e$ is the variation of the α_{ab} component of the polarization tensor for the vibration with normal coordinates q_e.

Symmetry considerations and group theory arguments define what are for each normal mode the polarizibility tensor components which have changed during the vibration. It can be easily shown that in the blende type crystals the two modes at the center of the Brillouin zone are Raman actives.

Experimental results giving the frequencies of the Raman active optical modes in blende structure are listed in Table IV.

Table IV

Observed frequencies of Raman active optical modes
in blende structure crystals.

	ω_{TO}	ω_{LO}	References
ZnS	274	349	a) L. Couture-Mathieu, J.P. Mathieu, C.R. Acad. Sci. Paris <u>236</u>, 371 (1953).
ZnSe	205	253	b) S.S. Mitra, J. Phys. Soc. Japan Suppl.<u>21</u>, 61 (1966)
	204	251	c) M. Krauzman, C.R. Acad. Sci. Paris <u>264</u>,1117 (1967)
	205	250	d) W. Taylor, Phys. Letters <u>24 A</u>, 556 (1967).
ZnTe	177	206	c) M. Krauzman, C.R.Acad.Sci. Paris <u>264</u>, 1117 (1967)
	174	203	d) W. Taylor, Phys. Letters <u>24 A</u>, 556 (1967).

4.2.2. Wurtzite.

Selection rules for Raman scattering in wurtzite structure crystals have also been deduced by group theory arguments [9]. The Raman active modes in wurtzite are the dollowing :

$$TO_{1\perp}(E_1) \; ; \; TO_{1//}(A_1) \; ; \; TO_2(E_2) \; ; \; TO_3(E_2) \; ; \; LO_{1\perp}(E_1) \; ; \; LO_{1//}(A_1) \quad .$$

In Table V are given the experimental results determining the frequencies of the Raman active modes in ZnO and CdS single crystals.

Table V
Observed frequencies for Raman active optical modes in wurtzite structure crystals.

	$\omega_{LO_1\perp}$	$\omega_{LO_1/\!/}$	ω_{TO_2}	$\omega_{TO_1\perp}$	$\omega_{TO_1/\!/}$	ω_{TO_3}	References
ZnO	583	574	437	407	380	101	a)
	538	588	383	438	420	180	b)
CdS		325	212	256		85	c)
	305	305	252	235	228	44	d)

References

a) T.C. Damen, S.P.S. Porto, and B. Tell, Phys. Rev. _142_, 570 (1966).
b) S.S. Mitra and J.I. Bryant, Bull. Am. Phys. Soc. _10_, 333 (1965).
c) H. Poulet and J.P. Mathieu, Ann. Phys. (Paris) _9_, 549 (1964).
d) B. Tell, T.C. Damen and S.P.S. Porto, Phys. Rev. _144_, 771 (1966).

Multiphonon Interaction.

The normal modes frequencies at the edges of the Brilluoin zone can be deduced from infrared absorption due to multiphonon interaction. Generally all phonons can participate to multiple processes ; the actual transitions obey selection rules deduced from symmetry considerations.

The theory of the interaction of the radiation field with two or more normal vibration modes has been given in terms of second or higher order dipole moments [10] or as due to the presence of anharmonic terms in the potential energy associated with lattice vibrations [11] and also as a combination of both [12].

In the case of optical absorption due to double-phonon processes, the contribution to the imaginary part of the dielectric constant due to anharmonic terms higher than second order in the potential energy can be written [13] :

$$\varepsilon''(\omega) = \pi^2 \chi \sum_{jj'} \int_{(\omega)} \left| \frac{a_T \, b_{jj'T}}{\omega_{TO}^2 - \omega_{jj'}^2} \right|^2 \frac{\bar{n}_{j'} + \frac{1}{2} \pm (\bar{n}_j + \frac{1}{2})}{\omega_j \omega_{j'} \, |\mathrm{grad}\, \omega(q)|_{\omega = \omega_{jj'}}} \, dq$$

$$+ \text{ higher order terms },$$

Here $a_T = e^*(N/M)^{1/2}$, $b_{jj'T} = \dfrac{\partial^3 \Phi}{\partial Q_j(q) \, \partial Q_{j'}(q') \, \partial Q_{TO}}$

is the coupling force between the TO mode and the phonons of wave
vector $q_j = \pm q_{j'}$, $\omega_{jj'} = \omega_j \pm \omega_{j'}$, $\bar{n}_j$ is the thermal mean value
of the quantum number n_j . The factors $(\bar{n}_j, +\bar{n}_j+1)$ and $(\bar{n}_j, -\bar{n}_j)$ give
the temperature dependence of the additive and subtractive absorption
bands.

The summation is taken over the surface $\omega(q)$ in the reduced
Brillouin zone for which $\omega(q) = \omega_{jj'}(q)$. The critical points for
this "combined" density of states give rise to bands in the absorp-
tion spectrum.

The contribution to the imaginary part of the dielectric con-
stant due to second or higher dipole moments can be written :

$$\varepsilon''(\omega) = \pi^2 \mathcal{M} \sum_{jj'} \int_{(\omega)} \left| \mathcal{M}\left(\begin{smallmatrix} q & -q \\ j & j' \end{smallmatrix}\right) \right|^2 \frac{\bar{n}_j, + \frac{1}{2} \pm (\bar{n}_j + \frac{1}{2})}{\omega_j \, \omega_{j'} \, |\mathrm{grad}\,\omega(q)|_{\omega=\omega_{jj'}}} \, dq$$

$$+ \text{ higher order terms.}$$

Here $\mathcal{M}\left(\begin{smallmatrix} q & -q \\ j & j' \end{smallmatrix}\right) = \delta^2\mathcal{M}/\delta Q\left(\begin{smallmatrix} q \\ j \end{smallmatrix}\right).\delta Q\left(\begin{smallmatrix} -q \\ j' \end{smallmatrix}\right)$ is the change of effective charge
associated with a given phonon $\left(\begin{smallmatrix} q \\ j \end{smallmatrix}\right)$ due to a second phonon $\left(\begin{smallmatrix} -q \\ j' \end{smallmatrix}\right)$.

Thus independently of the nature of the processes with which
one is concerned the characteristic variation of the absorption coef-
ficient as a function of the temperature is the same.

Analysis of the absorption bands in the infrared studied as a
function of the temperature allows to find the critical points of the
combined density of states. It should be mentionel that this critical
points do not have to correspond always to the critical points for the
density of states for simple phonons. The condition $\mathrm{grad}\,\omega(q) = 0$
can be satisfyed when $\mathrm{grad}\,\omega\left(\begin{smallmatrix} q \\ j \end{smallmatrix}\right) = \pm \mathrm{grad}\,\omega\left(\begin{smallmatrix} q \\ j' \end{smallmatrix}\right)$ with + for subtrac-
tive and - for additive processes which correspond to equal and op-
posite of sign slops of the two-phonon branches. It is also satisfied
when $\mathrm{grad}\,\omega\left(\begin{smallmatrix} q \\ j \end{smallmatrix}\right) = \mathrm{grad}\,\omega\left(\begin{smallmatrix} q \\ j' \end{smallmatrix}\right) = 0$ which corresponds to critical points
of the density of states curve for simple phonons.

It cannot be distinguished between this two cases experimentally.
It is then necessary to perform the calculation of the dispersion
curves on the basis of a given model and calculate afterwards the
hystogram of the double-phonon density of states and compare this
hystogram to the experimental curve. In the case of a rigid ion model
for CdS this work has been done recently by Nusimovici and Birman [6].
The qualitative agreement between the two curves is satisfactory. This
analysis shows also that all the early works on multiphonon spectra
implies a great part of arbitrary assignments.

In Fig.17 are presented on the same frequency scale the two-phonon density of states and the absorption spectrum corresponding to double-phonon transitions in CdS.
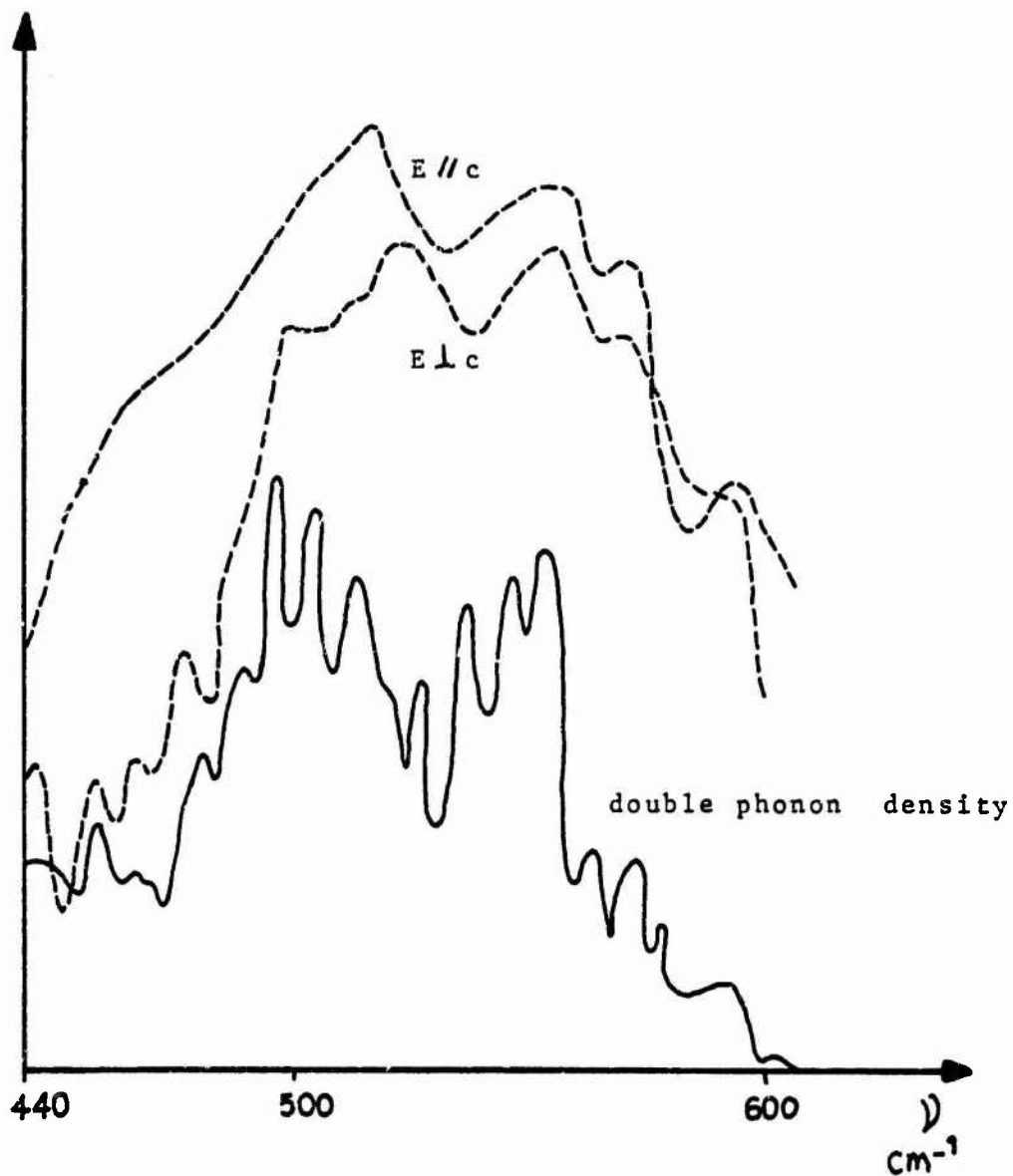
Figure 17. Comparison between the calculated and the experimental double phonon densities.

5. Localized Modes of Vibrations.

5.1. Localized Surface Modes.

For a finite crystal the surface atoms vibrates in a manner different from the atoms in the volume. Wallis [14] has studied diatomic cubic crystals and find that in addition to the normal modes of vibrations it appears localized surface modes whose frequencies are situated in the forbidden frequency gap between the acoustical and optical bands. The surface modes have non-vanishing electric dipole moments and may give rise to infrared absorption. Such absorption has not yet been observed experimentally.

In order to be able to observe localized surface modes it is necessary that the ratio surface/volume is as large as possible. If one considers thin film samples the surface atoms can be seen as independent impurities atoms. There are approximatively 10^{14} atoms per cm^2 at the surface and for a layer of thickness d this would correspond to $10^{14}/d$ per cm^3 impurity atoms. Localized modes for impurities become observable for concentration of the order of 10^{18} cm^{-3} and this means that surface modes can be observed in thin films of thickness $d \ll 1\,\mu$.

5.2. Localized modes of vibrations due to impurity atoms in II-VI compounds.

Localized modes have been observed by means of infrared spectroscopy in homopolar semiconductors like Si containing light impurities[15], in intermetallic semiconductors like GaAs with Li and P [16,17] and InSb with Al [18], as well as in ionic crystals [19]. The frequencies of the localized modes due to substitutional atoms and their coupling with the radiation field can be deduced on the basis of simple theory [20] when no changes in force constant are involved.

Some semiconductor crystals of the II-VI group such as ZnSe and CdS doped with Li and Al [21] have been investigated recently. Infrared absorption due to localized vibrations in CdSe containing S and CdTe containing Se and Li has also been investigated [22]. Here the frequencies of the absorption peaks attributed to localized modes are compared with that calculated for a mass defect in wurtzite CdS [23] subject to appropriate normal modes frequency scaling.

5.2.1. Theoretical considerations.

The perfect lattice vibrational frequencies ω are roots of the secular equation

$$\text{Det } |M\omega^2 - \Phi| = 0 \tag{5.1}$$

where Φ is the potential energy matrix for the perfect crystal formed by atoms with mass M. The introduction of an imperfection into the crystal brings a perturbation c to the potential energy. The matrix representing the potential energy of vibration of the crystal with impurities is $\Phi + c$. The secular equation for the perturbed crystal is then

$$\text{Det } |M\omega^2 - \Phi - c| = 0 \quad . \tag{5.2}$$

It is possible to define a matrix g whose coefficients are the Green's functions of the crystal :

$$g(M\omega^2 - \Phi - c) = 1 - gc \quad . \tag{5.3}$$

The localized modes, due to presence of impurities, are then solutions of the secular equation

$$\text{Det } |1 - g(\omega)\, c(\omega)| = 0 \quad . \tag{5.4}$$

In the wurtzite structure CdS the unit cell 1 contains four atoms $k = 1, 2, 3, 4$ which are respectively Cd_I, Cd_{II}, S_I, S_{II} . We just consider a single mass defect (the force constants are left unchanged). The defect subspace is three dimensional and localized mode frequency is a solution of the secular equation (5.4).

The matrix $\underline{c}$ is a unit three dimensional matrix multiplied by $(M_k - M')\omega^2$ where M' is the impurity mass and M_k the mass of the replaced host ion.

The matrix $\underline{g}$ Green's functions elements are deduced from the phonon eigenvectors $\underline{\sigma}(j\underline{q})$ and eigenfrequencies $\omega^2(j\underline{q})$:

$$g_{\alpha k, \alpha' k'}(1,1')(\omega^2) = \sum_{j\underline{q}} \frac{\sigma_{\alpha k}(j\underline{q})\, \sigma^+_{\alpha' k'}(j\underline{q})\, \exp i\underline{q}(r_1 - r_1')}{N\, M_k^{1/2}\, M_{k'}^{1/2}\, [\omega^2 - \omega^2(j\underline{q})]} \quad . \tag{5.5}$$

From the point group symmetry of the crystal around the defect the Green's functions satisfy the following relations :

$$g_{\alpha k, \alpha' k'}(0,0)(\omega^2) = \delta_{\alpha\alpha'} \; g_{\alpha k, \alpha k}(0,0)(\omega^2)$$

and

$$g_{xk, xk}(0,0)(\omega^2) = g_{yk, yk}(0,0)(\omega^2) \; .$$

(5.6)

The impurity may replace either Cd or S and four different Green's functions are used in this problem :

$$
\begin{aligned}
g_1 &= M_1 \; g_{z1, z1}(0,0)(\omega^2) \; , \\
g_2 &= M_1 \; g_{x1, x1}(0,0)(\omega^2) \; , \\
g_3 &= M_3 \; g_{z3, z3}(0,0)(\omega^2) \; , \\
g_4 &= M_3 \; g_{x3, x3}(0,0)(\omega^2)
\end{aligned}
$$

(5.7)

where M_1 and M_3 are respectively the mass of Cd and the mass of S.

For many defect vibration problems and especially for band resonance calculations it is convenient to know

$$\lim_{\varphi \to 0} g(\omega \pm i\varphi) = g'(\omega) + \frac{i\pi}{2\omega} \nu(\omega) \; . \tag{5.8}$$

The values of

$$\nu_{\alpha k, \alpha' k'}(1,1')(\omega) = \frac{1}{N} \sum_{j\underline{q}} \sigma_{\alpha k}(j\underline{q}) \; \sigma^{+}_{\alpha' k'}(j\underline{q}) \; \exp i\underline{q}(r_l - r_{l'}) \; \delta[\omega(j\underline{q}) - \omega] \tag{5.9}$$

are obtained by using the computed CdS spectrum [4] for 125 values of $\underline{q}$ in the reduced Brillouin zone. The frequency band ($\omega < \omega_M$) is divided into $Z = 61$ equally spaced regions and the sum (5.9) carried over $m(\omega_M/Z) < \omega < (m+1)(\omega_M/Z)$ to from a hystogram for ν. The values of $g'(\omega)$ are then obtained at the mid points of the hystogram sections by using the Kramers-Krönig relation
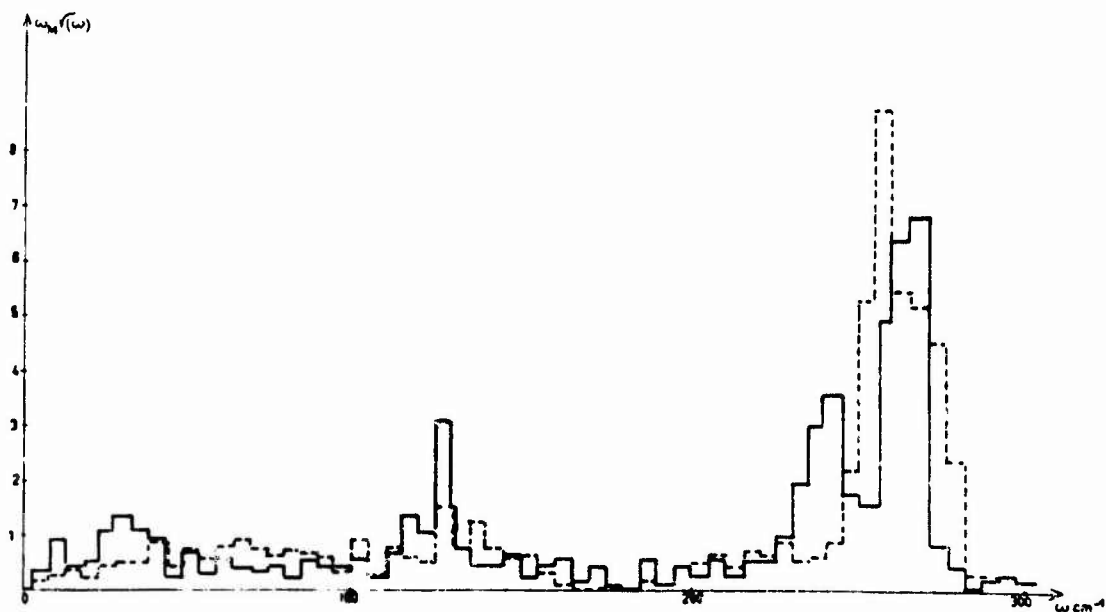
$$g'_i(\omega) = \int_0^{\omega_M} \frac{\nu_i(\omega') \; d\omega'}{\omega^2 - \omega'^2} \; .$$

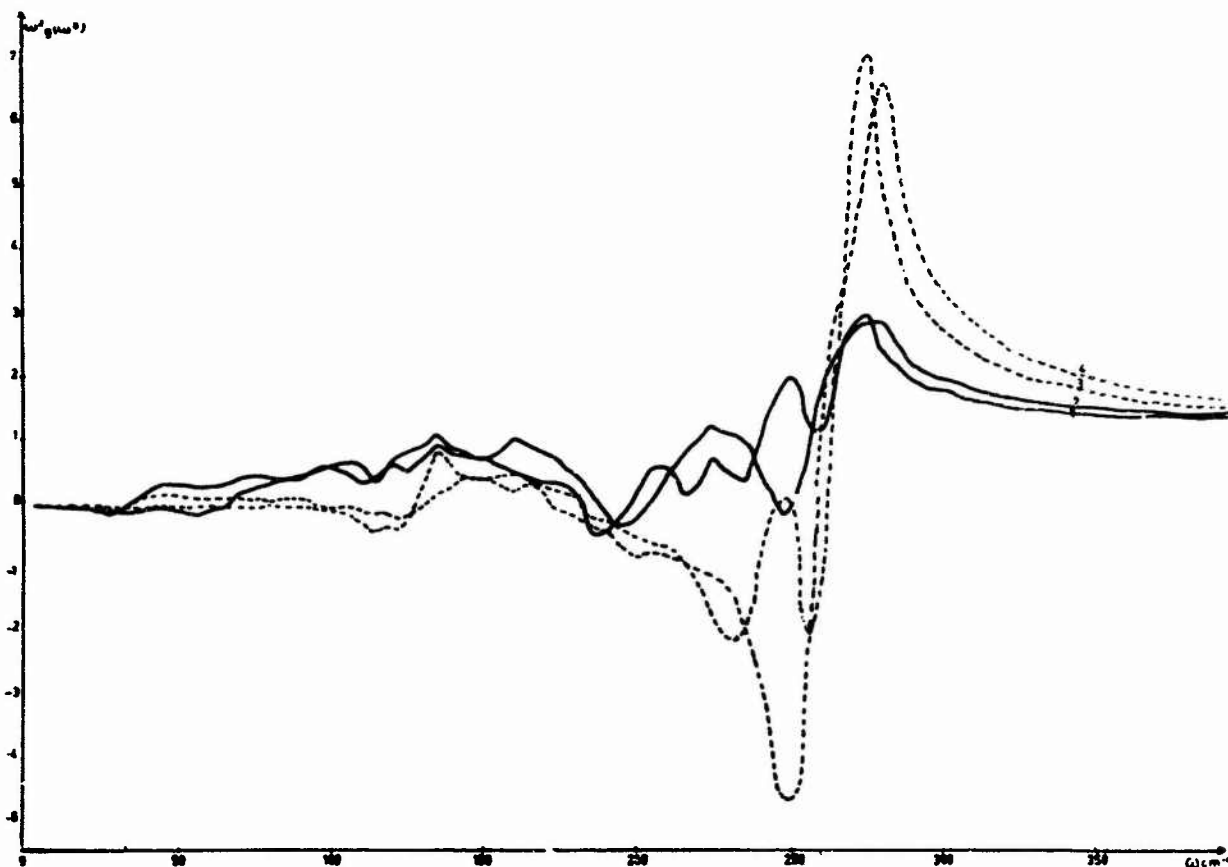The results for $\omega_M \nu_i(\omega)$ and for $\omega^2 g_i^!(\omega)$ are plotted in Figs. 18, 19 and 20.
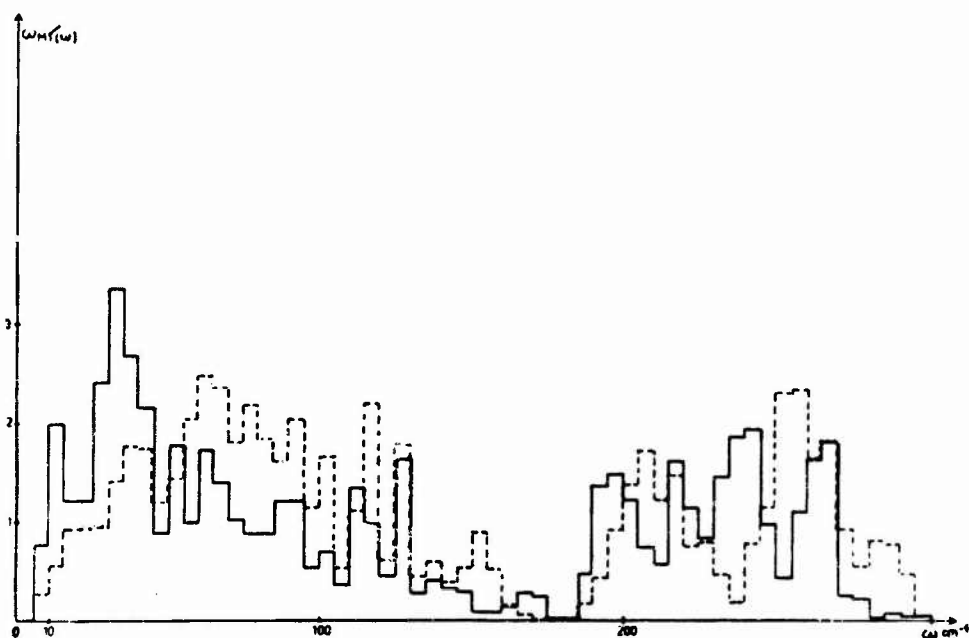
Figure 18. Imaginary part of the Green's functions.
$\omega_M \nu_1$ (ω) corresponds to curve 1: $\,$ ------
$\omega_M \nu_2$ (ω) corresponds to curve 2: ———

Figure 19. Imaginary part of the Green's functions.
$\omega_M \nu_3$ (ω) corresponds to curve 3: $\,$ ------
$\omega_M \nu_4$ (ω) corresponds to curve 4: ———

Figure 20. Real part of the Green's functions.
$\omega^2 g'_1(\omega)$ corresponds to curve 1, $\omega^2 g'_2(\omega)$ to curve 2,
$\omega^2 g'_3(\omega)$ to curve 3, and $\omega^2 g'_4(\omega)$ to curve 4.

The localized mode frequencies are solutions of the following equations :

$$\varepsilon_1 \, \omega^2 \, g_1 = 1 \quad \text{for the } \Gamma_1 \text{ mode}$$
$$\varepsilon_1 \, \omega^2 \, g_2 = 1 \quad \text{for the } \Gamma_5 \text{ mode}$$

(5.10)

where the impurity replaces Cd and

$$\varepsilon_3 \, \omega^2 \, g_3 = 1 \quad \text{for the } \Gamma_1 \text{ mode}$$
$$\varepsilon_3 \, \omega^2 \, g_4 = 1 \quad \text{for the } \Gamma_5 \text{ mode}$$

(5.11)

where the impurity replaces S

$$\varepsilon_1 = (M_1 - M')/M_1 \quad \text{and} \quad \varepsilon_3 = (M_3 - M')/M_3 \quad .$$

The imaginary part of the Green's functions $v_i(\omega)$ may be compared with the one-phonon density of states in CdS recently calculated[6] and shown in Fig.21. The functions $v_1(\omega)$ and $v_2(\omega)$ related to the heavy Cd ion displacement vectors are enhanced in the low frequency acoustic region and the functions $v_3(\omega)$ and $v_4(\omega)$ related to the light S ion displacement vectors are enhanced in the high frequency optic region.
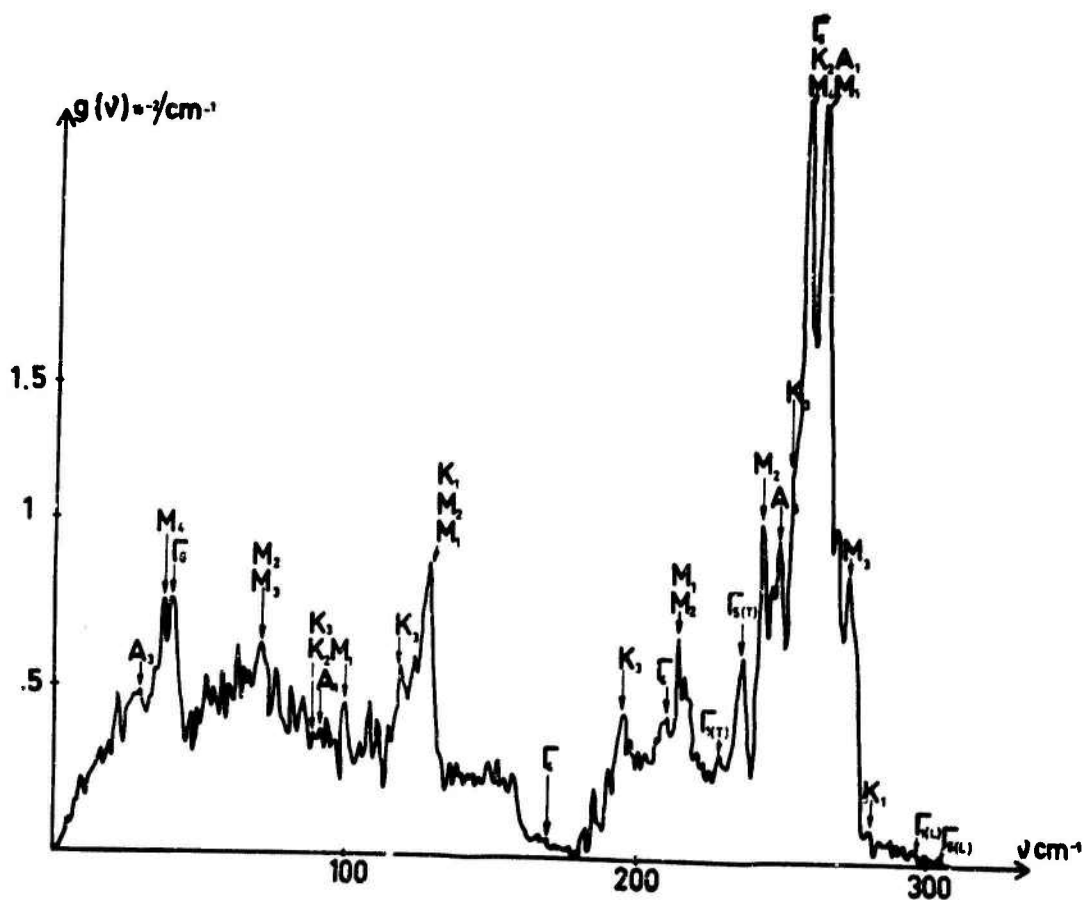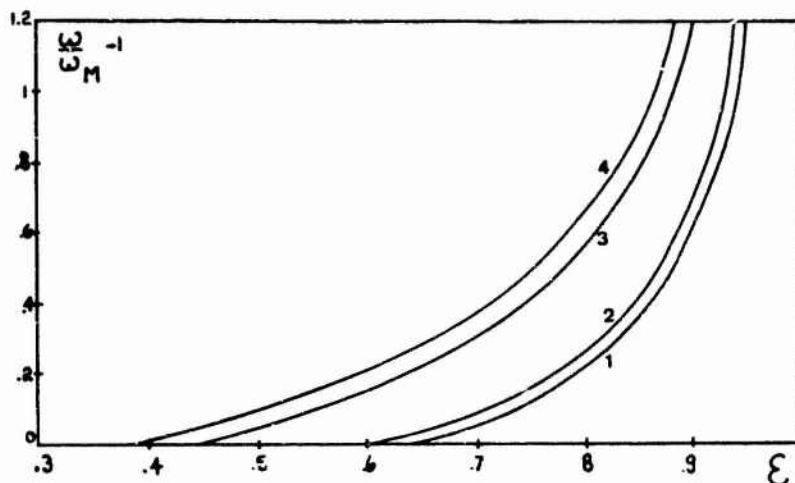

Figure 21.   One phonon density of states for CdS.

a) Localized Modes.

The localized mode frequencies obtained from equations (5.10) and (5.11) are plotted in Fig.22 versus ε.

Figure 22. Localized mode frequencies for a mass defect $\frac{\omega}{\omega_M} - 1$ is plotted versus ε_1 for curves 1 and 2 where the impurity replaces Cd, and versus ε_3 for curves 3 and 4 where the impurity replaces S. Curves 1 and 3 correspond to Γ_1 modes and curves 2 and 4 to Γ_5 modes.

If we suppose $\omega_M = 308$ cm^{-1} for CdS a localized mode appears only if $\varepsilon_3 > 0.36$ for an impurity replacing S and $\varepsilon_1 > 0.58$ for an impurity replacing Cd. If ε is large enough, two modes appear out of the band; a singlet Γ_1 and a doublet Γ_5 with a higher frequency than the singlet. The splitting increases when the impurity becomes lighter. Up to now localized modes due to a light impurity mass defect have only been observed for Li^6 and Li^7 in CdS [21]. We shal discuss such modes observed in other II-VI semiconductors. Predictions for different impurities in CdS are summarized in Table VI.

Table VI

Localized mode frequencies for substitutional
impurities in CdS

Impurity	Replaced Ion	M^1	ε	$\omega\Gamma_1$ cm^{-1}	$\omega\Gamma_5$ cm^{-1}
Be	Cd	9	0.92	540	580
Mg	Cd	24	0.786	365	380
Ca	Cd	40	0.683	320	330
O	S	16	0.5	324	339
Li	Cd	7	0.94	615	665

For light impurities ($\varepsilon \to 1$) all the localized mode frequencies tend to infinity. This can be shown from the limit form of the Green's functions vhen ω is much bigger than $\omega(j\underline{q})$:

$$g_{\alpha k, \alpha k}(0,0)(\omega^2) \sim \sum_{j\underline{q}} \frac{|\sigma_{\alpha k}(j\underline{q})|^2}{N} \frac{1}{M_k \omega^2} \quad ,$$

but

$$\sum_j \sigma_{\alpha k}(j\underline{q}) \; \sigma^+_{\beta k'}(j\underline{q}) = \delta_{\alpha\beta} \; \delta_{kk'} \quad ,$$

then when $\omega \to \infty$

$$g_{\alpha k, \alpha k}(0,0)(\omega^2) \longrightarrow \frac{1}{M_k \omega^2}$$

and the solution for ε is $\varepsilon = 1$.

b) Band Modes.

When a heavy mass impurity is introduced a band resonance may appear at $\omega < \omega_M$. The response of the lattice is related to the imaginary part of the imperfect crystal Green's functions

$$\text{Im } g_i(\omega) = \frac{[\pi \nu_i(\omega)]/2\omega}{[1 - \varepsilon\omega^2 g_i'(\omega)]^2 + [\pi\varepsilon\omega\nu_i(\omega)]^2/2} \quad .$$

So a resonance is well defined at the ω which is a solution of $1 - \varepsilon\omega^2 g_i'(\omega) = 0$ only if $\nu_i(\omega)$ is small. For Se in CdS, $\varepsilon = -1.5$ and a resonance is expected at 210 cm^{-1} .

The model on which this calculation is based being simple, one is justified to extend the results to other II-VI compounds when no considerable changes in force constants are expected when going from one compound to another.

In the cubic crystals of this group, like CdTe for example, the site symmetry is T_d and therefore one triply degenerate mode Γ_5 is to be expected.

5.2.2. Experimental observations of localized band and gap modes.

5.2.2.1. Se in CdS.

When introduced in CdS single crystals the Se with mass $M = 79$ replaces the S atom with mass $m_2 = 32$, Cd having a mass of $m_1 = 112.4$, we have the relation $m_2 < M < m_1$. The mass parameter in this case is $\varepsilon = (m_1 - M)/m_1 = -1.47$. The infrared reflectivity spectrum (Fig.23) of this system shows a resonance at 180 cm^{-1}.
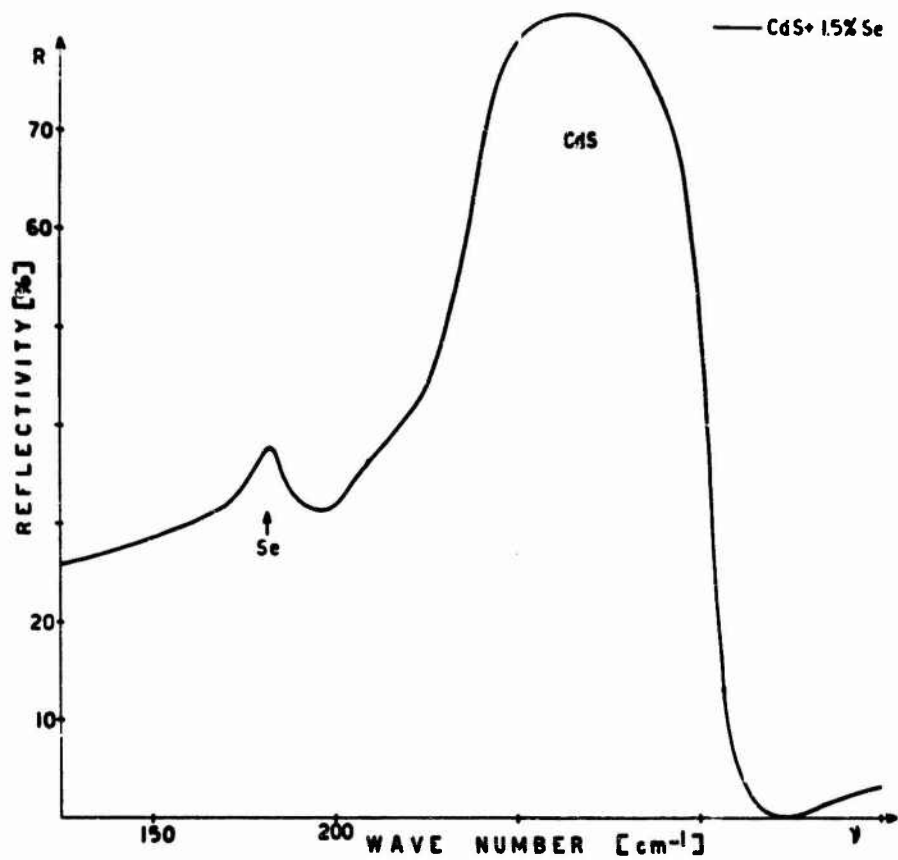

Figure 23.   Infrared reflectivity spectrum of CdS with 1.5 % Se.

This frequency being out of the restrahlen region the corresponding
mode could be considered as a gap mode. The density of mode at this
frequency (see Fig.21) is very low, practically zero, one can there-
fore consider that this mode is situated in a forbidden frequency
region , the frequency gap , and is therefore called a gap mode.
With increasing concentration of Se the gap mode frequency, ω_g = 180
cm^{-1}, splits off into two modes having respectively the characters
of a transverse optical and a longitudinal optical modes.The frequen-
cies of these two modes fall apart from each other linearly with the
concentration and reach the limit of ω_{TO} and ω_{LO} for CdSe respectively
ω_{TO} = 170 cm^{-1} and ω_{LO} = 210 cm^{-1} when Se approaches 50%. The varia-
tions of ω_{LO} and ω_{TO} deduced from the position of each concentration
of crossing of the zero line for the real part of the dielectric con-
stant in changing from negative to positive values and from the posi-
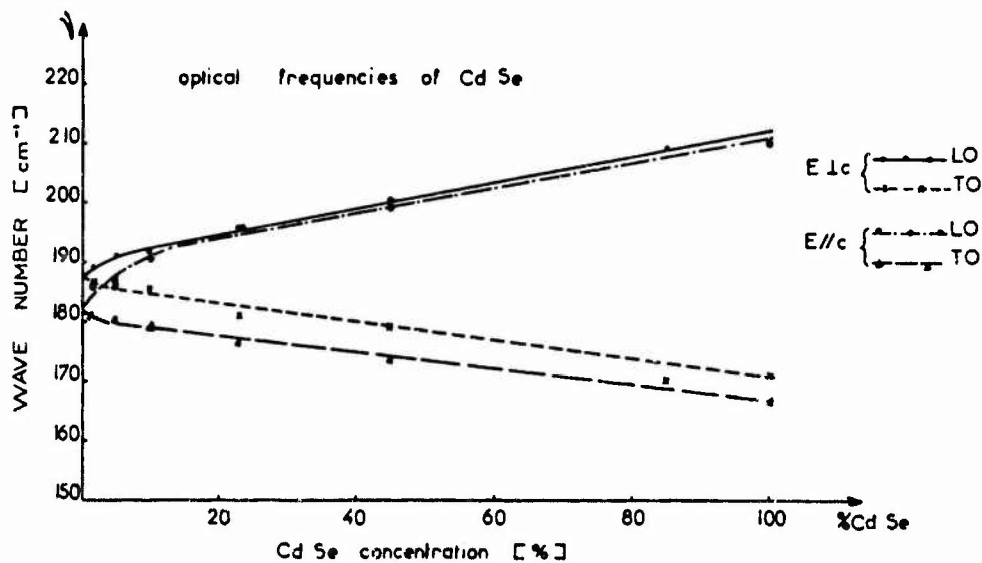tion of the peak of the imaginary part of the dielectric constant are
shown in Fig.24.

Figure 24.   Frequency variation of TO and LO in the CdS-Se alloy
with increasing concentration of Se.

In earlier investigations [24]   concerning the reflectivity
spectra of CdS-Se alloys analogous results have been obtained.

5.2.2.2. S in CdSe.

For concentration higher than 50% of Se in CdS the situation will be inverted, the impurity will be now S in CdSe. S is a light impurity $M = 32$ in CdSe substituting Se with $m_2 = 79$, the defect mass parameter ε here is $E = (79-32)/79 = 0.595$.

In the wurtzite structure CdS have a unit cell 1 containing four atoms $k = 1, 2, 3, 4$, which are respectively Cd_I, Cd_{II}, S_I and S_{II}. The point defect introduced in the perfect crystal substitutes one of these atoms. In a first approximation only the mass defect is considered assuming that substitution of an atom for another does not introduce changes in the force constants of the perfect crystal. The localized mode frequency is a solution of the secular equation (5.4). To solve this equation it is necessary to take only a 3×3 submatrix $G(\omega^2)$ corresponding to the defect subspace. Substitution of the Cd and S atoms are studied with the mass coefficients respectively

$$\varepsilon_1 = \Delta M/M_1 \quad , \quad \varepsilon_3 = \Delta M/M_3 \quad .$$

In the wurtzite crystal the point defect has no more the site symmetry Γ_D but C_{6v} and the triply degenerate localized mode Γ_{15} is now split into two modes Γ_1 and Γ_5 simply and doubly degenerate. The localized mode frequencies are solutions of the following equations when the impurity replaces Cd atoms :

. $\varepsilon_1 \omega^2 g_2 = 1$ for the Γ_5 mode doubly degenerate corresponding to vibrations of the impurity atoms perpendicular to the c axis of the crystal ;

. $\varepsilon_1 \omega^2 g_1 = 1$ for the Γ_1 mode non-degenerate corresponding to vibrations of the impurity atoms parallel to the c axis of the crystal.

When the impurity replaces the S atoms the localized mode frequencies are solutions of the following equations :

$$\varepsilon_3 \omega^2 g_4 = 1 \quad \text{for the } \Gamma_5 \text{ mode },$$
$$\varepsilon_3 \omega^2 g_3 = 1 \quad \text{for the } \Gamma_1 \text{ mode.}$$

The position of the localized modes is obtained directly according to these equations from the plot of $\omega^2 g(\omega^2)$ as a function of the frequency in taking $\omega^2 g(\omega^2) = \frac{1}{\varepsilon}$.

If we admit that the density of states does not considerably changes from CdS to CdSe we may then use the calculated curve for CdS given in Fig.22, provide we make the appropriate frequency scaling in substituting for ω_M the value of ω_{LO} for CdSe which is $\omega_{LO} = 210$ cm^{-1}, to deduce ω_1 . The values obtained in this way are $\omega_1(\Gamma_1) = 244$ cm^{-1} and $\omega_1(\Gamma_5) = 256$ cm^{-1}. The infrared reflectivity spectrum for CdSe containing S is given in Fig.25.
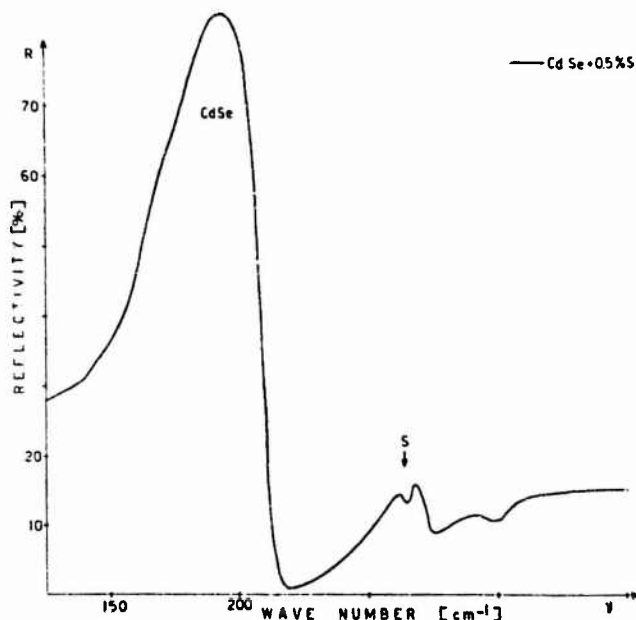

Figure 25.   Infrared reflectivity of CdSe with 0.5 %S.

The experimental values deduced from Fig.25 are respectively $\omega(\Gamma_1) = 266.5\ cm^{-1}$ and $\omega(\Gamma_5) = 269\ cm^{-1}$.

The difference between the calculated and observed values could be attributed to a decrease of the first neighbours force constants when S is substituted for Se.

The line width is of the order of 4 cm^{-1} and the relative line width $\Delta\omega/\omega = 0.015$ which is of the order of magnitude for relative broadening   when $\Delta\omega$ describes the broadening of an optical spectral line due to anharmonic interaction involving the vibrational energy of the local mode. A temperature line shift is observed of the order of 3 cm^{-1} between 25°K and 300°K.

On the basis of symmetry consideration it is easy to deduce the selection rules showing that from the split of Γ_1 and Γ_5 modes only one will be optically active for polarized light. The Γ_1 will be active for light with E//C and Γ_5 will be active for E⊥C. It is surprising to find out that experimentally the two picks seem to be optically active.

When the concentration of S in CdSe increases the two localized modes shifts in frequency until reaching the limit frequencies corresponding to the normal modes in CdS respectively $\omega_{TO} = 240$ cm^{-1} and $\omega_{LO} = 300$ cm^{-1}.

6.2.2.3. Light impurities in CdTe.

CdTe has the cubic zinc-blende (sphalerite) structure band on the cubic space group T_d^2. The dispersion curves calculated for a hypothetical cubic CdS show only slight difference from that of wurtzite. If it is acceptable to use the same frequency distribution as in CdS it will be possible with an appropriate frequency scaling for LO to deduce a value for ω_l for each impurity. The frequency of the localized mode obtained in this way may represent a good order of magnitude to compare with the exprimental results.

a) Se in CdTe.

Se M = 79 is a light impurity in CdTe which substitutes to the Te atom whose mass is $m_2 = 127.6$. The mass parameter in this case is E = 0.38. The longitudinal optical mode frequency is $\omega_{LO} = 167$ cm^{-1}. From the relations given in Fig.22 it is easy to deduce the value of the localized mode frequency which is $\omega_l = 167$ cm^{-1}.

The infrared reflectivity spectrum for CdTe containing Se is given in Fig.26.
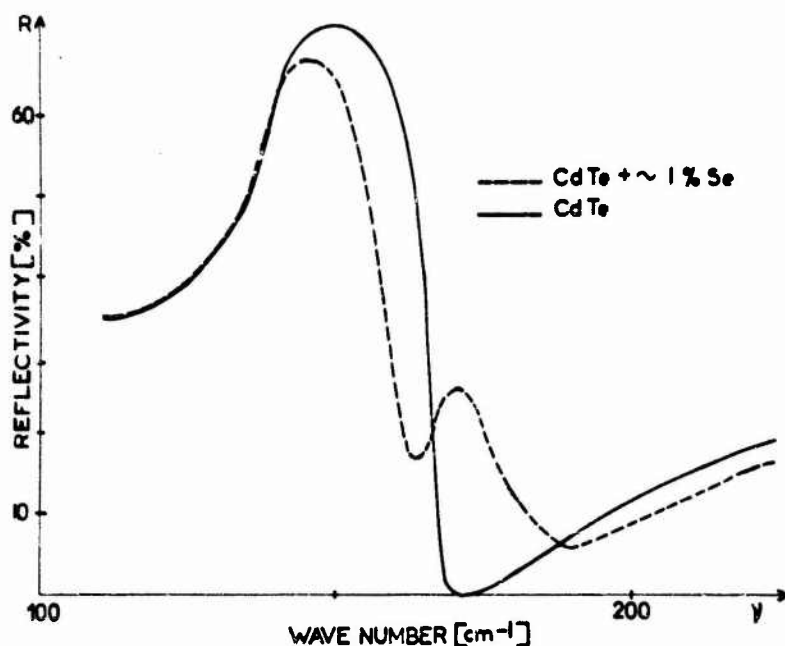
Figure 26. Infrared reflectivity spectrum of CdTe with $\sim$ 1 % Se.

The Kramers-Krönig analysis of the optical constants is represented graphically in Fig.27.
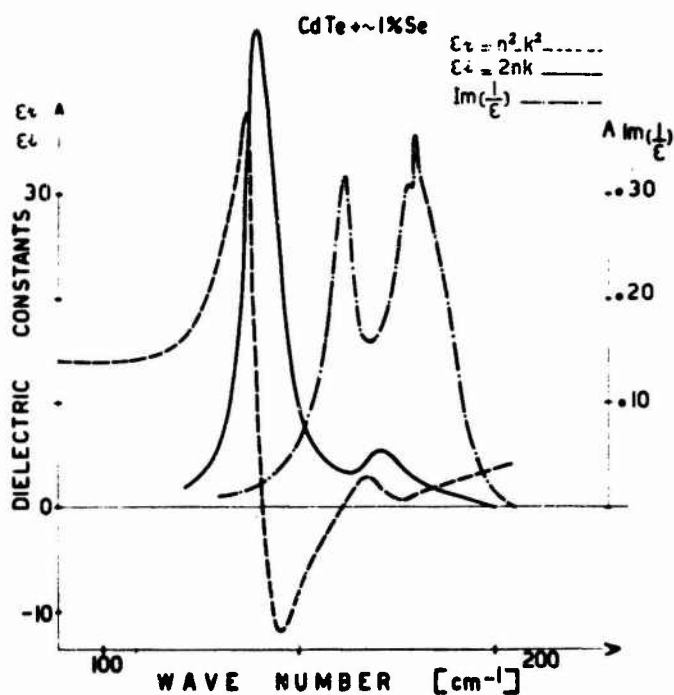

Figure 27. Dielectric constants of CdTe with $\sim 1\%$ Se.

From the peaks of the imaginary parts of the dielectric constant we deduce the values of $\omega_{TO} = 139 \text{ cm}^{-1}$ and the localized mode frequency $\omega_1 = 170 \text{ cm}^{-1}$. The calculated $\text{Im} \frac{1}{\varepsilon}$ shows two peaks at frequencies 162 and 180 cm^{-1}. For pure CdTe the longitudinal optical mode frequency is $\omega_{LO} = 167 \text{ cm}^{-1}$; in doped crystals we have $\omega_{LO} = 162 \text{ cm}^{-1}$ and $\omega_1^{LO} = 180 \text{ cm}^{-1}$; ω_{LO} would then suffer a slight shift of 5 cm^{-1} when a light impurity is introduced.

The line width for ω_1 is of the order of 10 cm^{-1} and the relative line width $\Delta\omega/\omega \simeq 0.059$ which can still be considered as relative anharmonic broadening.

b) Li in CdTe.

The introduction of Li in CdTe has been done by the method of progressive crystallization. The crystals obtained by this method when at low concentration of Li approximately 0.1% are n-type and with low free carrier concentration of the order of $8 \times 10^{14} \text{ cm}^{-3}$. At higher Li concentration approximately 1% the samples are of p-type, the free carrier concentration is very low of the order of $5 \times 10^{13} \text{cm}^{-3}$.

The samples with low Li concentration are opaque in the infrared. At higher Li concentration the samples become transparent probably because of a partial compensation.

At low concentration Li is supposed to occupy interstitial sites and to act as a donor whereas at high concentration the occupation of substitutional sites where Li acts as an acceptor becomes predominant. In the neighbourhood of 1% of Li a partial compensation is achieved and the samples are transparent. The absorption spectra of crystals with 1% of Li at 300°K and 100°K are given in Fig.28.
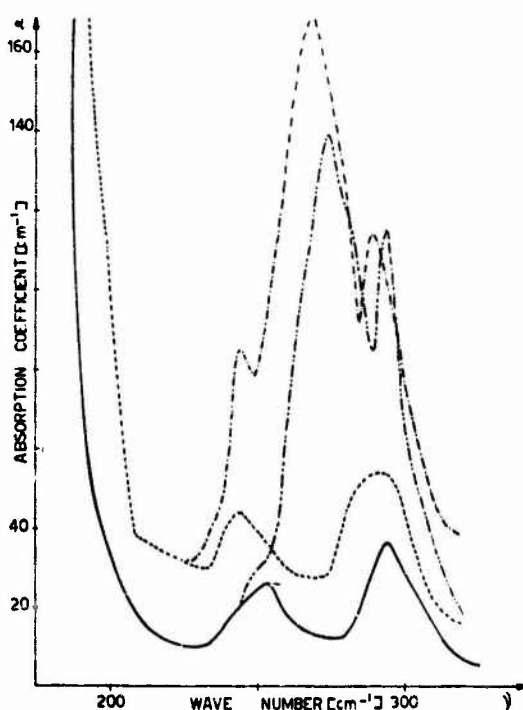

Figure 28.   Absorption spectra of CdTe with 1 % Li at 300°K

Pure crystal   ------------

1 % Li   — . — . —

and at 100°K

Pure crystal   ——————

1 % Li   — .. — .. —

These spectra clearly show absorption peaks due to the presence of Li. The largest peak is centered at 270 cm^{-1} at 300°K and it shifts toward the high frequency for lower temperatures : the maximum of the peak is situated at 275 cm^{-1} when taken at 100°K and it is at 277 cm^{-1} at 25°K.

The width of this band of the order of 35 cm^{-1} is anormally large so is also the relative band width $\Delta\omega/\omega = 0.130$.

5.2.2.4. Impurities in ZnSe.

ZnSe is again a cubic zinc-blende crystal for which the analysis of the infrared spectra concerning the phonon interaction with the radiation field can be treated on the basis of the equivalent dispersion relation for the sphalerite CdS. The tacite assumption in calculation the local mode frequencies ω_1 is that the frequency distribution is analogous to that of CdS. The experimental results are very close to that calculated in this hypothesis which can be therefore considered as a satisfactory first order approximation.

a) Mn in ZnSe.

When Mn, $M = 55$, is introduced in ZnSe it substitutes the Zn atom of mass $m_1 = 65.4$. The mass parameter is then $\varepsilon = 0.16$. The mass difference being extremely small $\varepsilon < 0.30$ for a $\omega_M = 252$ cm^{-1} the mode due to the presence of this impurity is a band mode and therefore not directly observable in the frequency range out of the restrahlen.

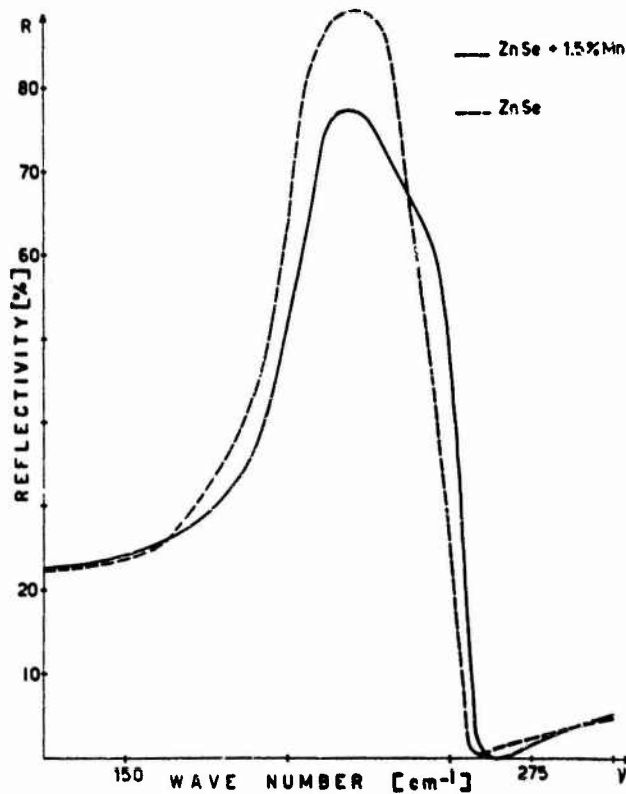The infrared reflectivity spectrum of this system is given in Fig. 29.

Figure 29.   Infrared reflectivity of ZnSe with 1.5 % Mn.

A close examen of the optical constants displayed in Fig.30 shows a structure on the imaginary part of the dielectric constant which gives two frequencies for the transverse optical mode : ω_1^{TO} = 19? cm^{-1} and ω_{TO} = 20? cm^{-1}.

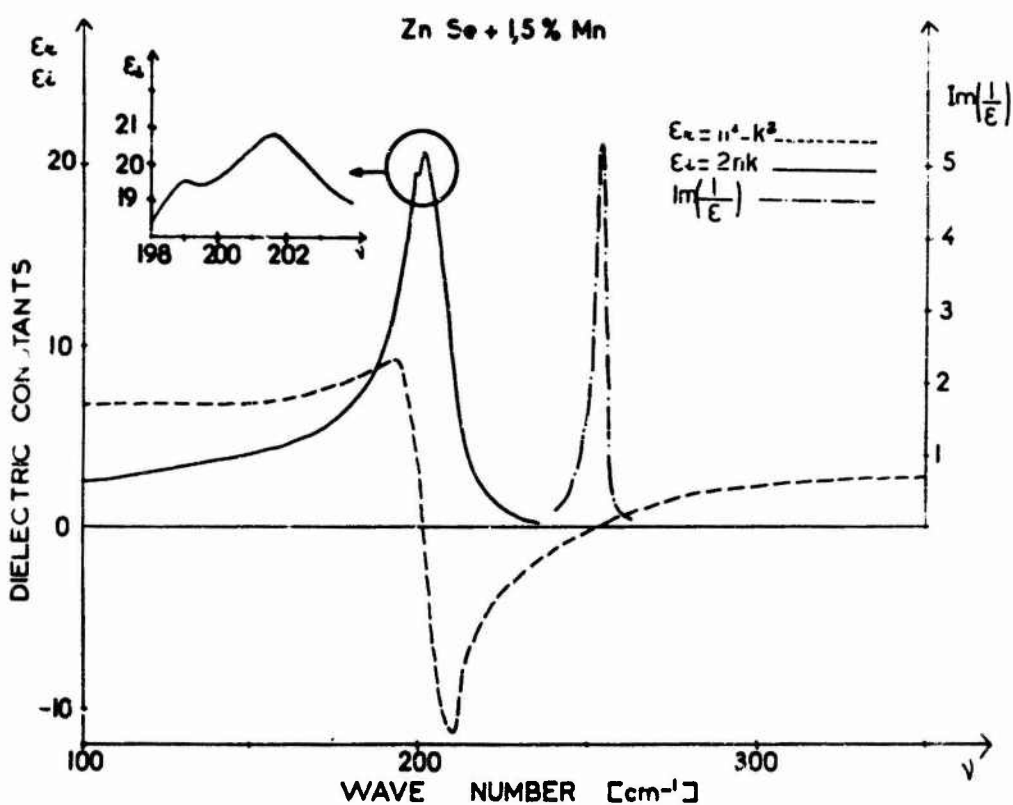**Figure 30.** Dielectric constants of ZnSe with 1.5 % Mn.

For the pure ZnSe we have ω_{TO} = 202 cm^{-1}. It seems that the presence cf an impurity shifts the ω_{LO} from ω_{LO} = 252 cm^{-1} to an higher energy ω_{LO} = 254 cm^{-1}

b) S in ZnSe.

S is a light impurity in ZnSe substituting Se. The mass factor is ε ÷ 0.595. The frequency scaling done with ω_{LO} = 252 cm^{-1} leads to a localized mode frequency ω_1 = 297 cm^{-1}.

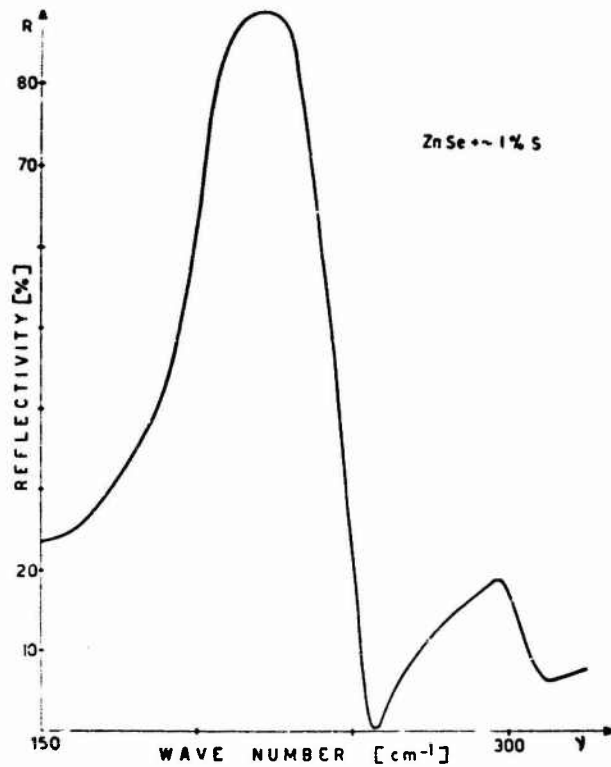The reflectivity spectrum for S doped ZnSe is represented in Fig.31.

Figure 31.   Infrared reflectivity of ZnSe with ~ 1 % S.

The real and imaginary parts of the dielectric constant deduced by the Kramers-Krönig analysis are desployed in Fig.32.
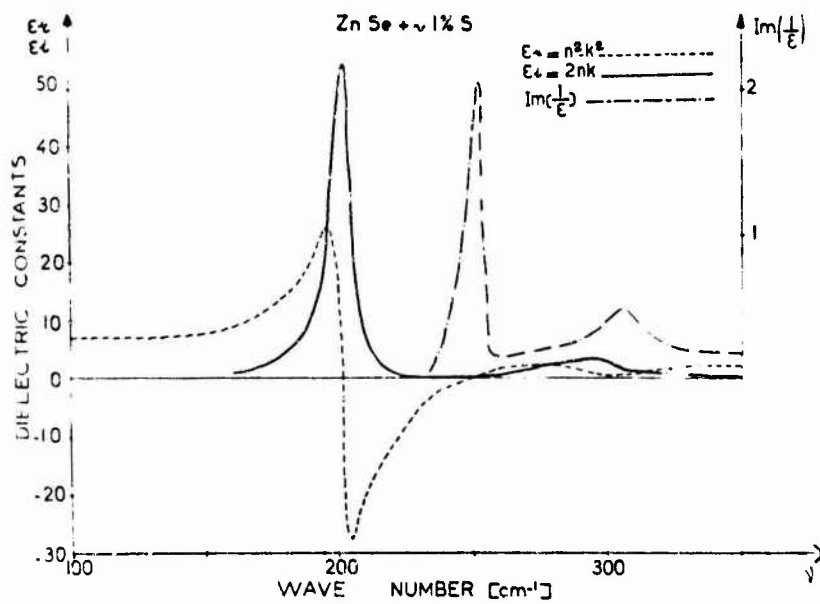

Figure 32.   Dielectric constants of ZnSe with ~ 1 % S.

The normal mode frequencies for the undoped crystal are $\omega_{LO} = 252$ cm^{-1}, $\omega_{TO} = 202$ cm^{-1}, and for the S doped the local mode frequencies are $\omega_1^{TO} = 297$ cm^{-1} and $\omega_1^{LO} = 305.5$ cm^{-1}.

The line width which is function of the concentration is in this case ($\sim$ 1% S) $\Delta\omega = 22$ cm^{-1} and the relative line broadening is $\Delta\omega/\omega = 0.074$.

c) <u>Te in ZnSe</u>.

Te with M = 127.6 is a heavy impurity in ZnSe. The mass parameter is $\varepsilon = -0.615$. A heavy defect in the lattice should lead to a resonance in the frequency allowed region or to a gap mode if the density of states at the given frequency is very low or pratically zero.

The infrared reflectivity spectra for pure and Te doped ZnSe are given in Fig.33.
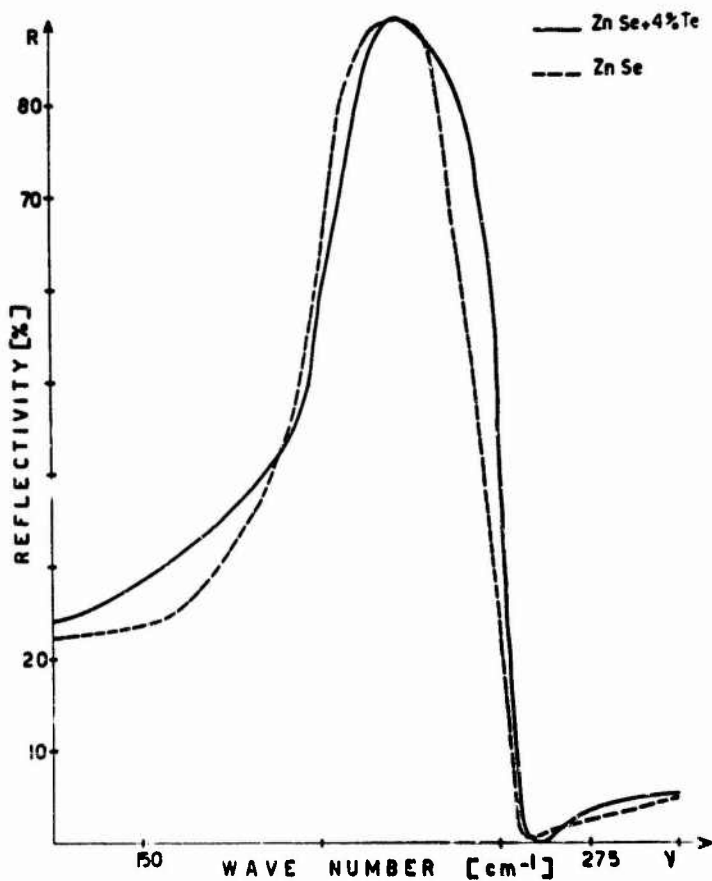
Figure 33.   Infrared reflectivity of ZnSe with 4 % Te.

The real and imaginary parts of the dielectric constant are desployed in Fig.34.
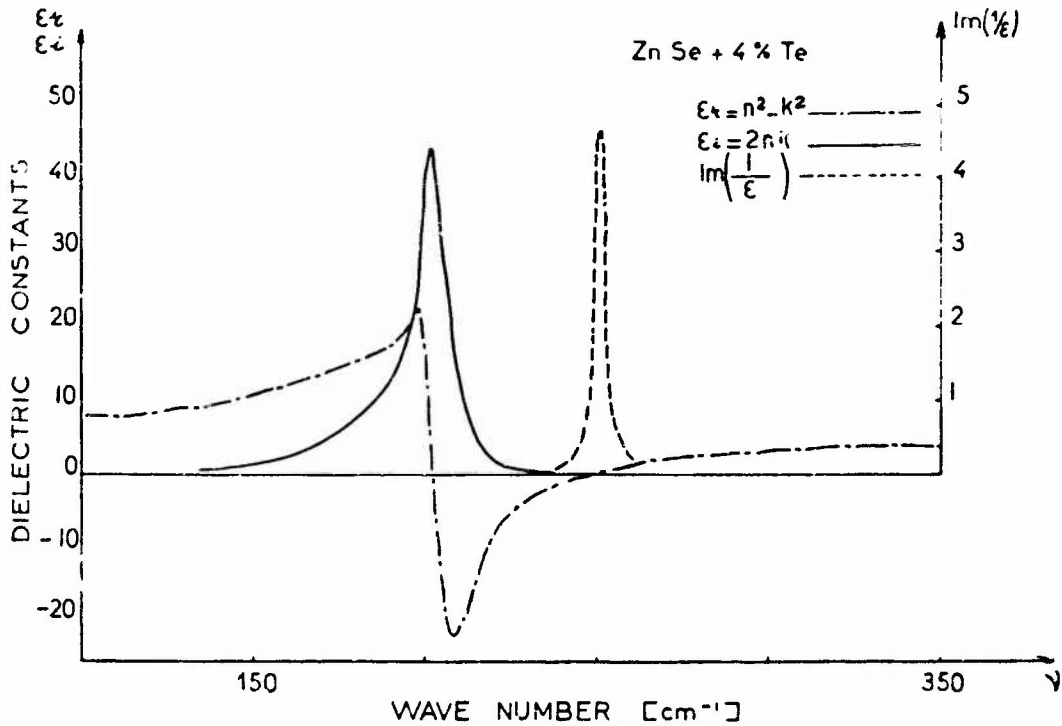
Figure 34.   Dielectric constants of ZnSe with 4 % Te.

From the difference between the imaginary part of the dielectric constant for pure ZnSe and Te doped ZnSe one can deduce the frequency of the gap mode ω_g = 182 cm^{-1}. The width of this band is $\Delta\omega$ = 40 cm^{-1} which combines the impurity line width and the band broadening due to the concentration. The relative band broadening is $\Delta\omega/\omega \simeq 0.22$.

7. Discussion.

In spite of the considerable amount of work presently under way in the lattice dynamics of the II-VI compounds and the considerable progress it still remains much to be done.

The dispersion relations for CdS have been calculated in terms of an extremely simplified model whose physical significance remains to be explicited. Although the first results are satisfactory and the eigenvalues and eigenfunctions have served as basis for the calculation of the local mode frequencies which are in good agreement with the experiment, it is certainly suitable to improve this model including physical parameter such as the electron polarizability of the ions. The calculated double-phonon density of states do not allow a direct comaprison with the two-phonon optical spectra in the whole spectral range. Such a descrepency should be understood eather in terms on unsatisfactory physical implications in the calculation of the frequency distribution curve or in terms of second order matrix elements for optical transitions employing more than two particles.

The qualitative features of the normal mode spectra are well understood and the spectral measurements give satisfactory quantitative data for those modes which are coupled to the radiation field at the appropriate points of the Brillouin zone which are eather the center or high symmetry edges.

Studies on thin films have proved to be extremely useful for the experimental determination of the normal mode frequencies.

Surface modes are still to be seen experimentally.

Elementary calculations using Green function technics and assuming isotopic substitution without force constant changes have proved to be an extremely useful guide in the discussion of the experimentally determined localized modes due to impurities. The orders of magnitude calculated even in drastic assumptions coincide very closely to with the experimentally measured values. The reason is probably the fact that the calculated density of states obtained in a very rough model which is used for the calculation of the localized modes frequencies is insensitive to slight changes in force contants when an ion is replaced with a similar ion from the same groups. Only an improved initial model may lead to results more sensitive on subtile force constant changes produced by the substitution of analogous ions.

The first measured localized mode frequencies in II-VI compounds are those concerning the Li doped ZnSe and CdS . In the case of CdS [21] doped with Li anormally large bands have been observed and attributed to the presence of Li^7 at 457 cm^{-1} and Li^6 at 474 cm^{-1}.

If Li was substituting Cd atom the mass difference parameter would be $\varepsilon = 0.938$ for Li^7 and $\varepsilon = 0.946$ for Li^6, this would give in the simplest approximation of isotopic mass substitution for the localized mode frequency of the impurity atom vibration along the c axis the following values :

for Li^7 , $\omega_{\Gamma_1} = 492$ cm^{-1} ,

for Li^6 , $\omega_{\Gamma_1} = 503$ cm^{-1} .

The calculated values are larger than that observed experimentally there would indicate that Li interacts stronger with the host lattice than a simple mass defect. A change of force constant would explain this difference. Increase in the deviation of force constant from the host lattice force constant acts in the same direction as a reduction of mass i.e. increase of the localized mode frequency.

The presence of S in CdSe crystals introduces a mass defect parameter $\varepsilon = 0.595$ and hence

$$\omega_{\Gamma_1} = 244 \; cm^{-1} \quad , \quad \omega_{\Gamma_5} = 256 \; cm^{-1} \quad .$$

Experimentally two peaks are observed at 266.5cm^{-1} and 269 cm^{-1} at room temperature. The calculated values now are smaller than the observed ones. This discrepency could be also attributed to a change in force constant where Se is replaced by S, in this case the substitution would means a decrease of force constant.

The line width is of the order of 4 cm^{-1} and the relative line width $\Delta\omega/\omega$ is 0.015 which is of the order of magnitude for relative broadening [25] of the defect mode frequency when $\Delta\omega$ describes the broadening due to anharmonic interaction of an optical spectral line involving the vibrational energy of the local mode.

A temperature line shift is observed of the order of 3 cm^{-1} between 25°K and 300°K.

In the case of Li doped CdTe an absorption band is observed centered at 270 cm^{-1} which could be attributed to localized modes due to the presence of Li but whose interpretation is difficult for many reasons and particularly because of the band width which is of the order of 35 cm^{-1} and does not seem to vary considerably with temperature. The relative band width $\Delta\omega/\omega$ here is 0.130 what is by a factor of 10 larger than what would be expected in the case of single substitutional impurity vibrations.

The essential contribution to the residual line width when $T \to 0$ comes from the contribution of the spontaneous decay of the excited localized vibrations into band modes. In this process the energy conservation principal $\sum \omega_k = \omega$ should be respected. In the case of Li in CdTe, as well as in the other cases we have examined here, $\omega < 2 \omega_m$, consequently the decay of a localized mode into two-band modes is possible through the third order anharmonic potential and this decay could be the dominant process at room temperature[26,27].

In order to understand the possibility to obtain optically transparent CdTe with relatively high concentration of Li we had to suppose that at low concentration Li is donor and at high concentration gives rise to acceptor levels. This leads to the possibility of an almost complete compensation for a given concentration of dopant. The interaction of an interstitial atom with the lattice is not the same as that on a substitutional impurity. It is therefore clear that although the mass is the same due to changes in the force constant the frequencies of the localized modes should be different for the two situations. One should in such a case observe two absorption peaks. In addition Li has two isotopes Li^6 and Li^7 constituting each one a mass defect and therefore giving rise to an absorption band each. All these are reasons to believe that the large band at 270 cm^{-1} contains a certain number of peaks remaining to be resolved in the simplest case.

Experiments are now undertaken at different concentrations of Li in order to further investigate this situation.

The presence of Se in CdTe leads to a typical localized mode whose frequency deduced from the Kramers-Krönig analysis of the reflectivity spectrum in $\omega_1 = 170$ cm^{-1} whereas the calculated value with the appropriate normal mode frequency scaling is $\omega_1 = 167$ cm^{-1}. The presence of impurities at relatively high concentration seems to have an effect on the longitudinal mode frequency which is expressed by a slight shift of the normal mode frequency ω_{LO} is now 162 cm^{-1} and a longitudinal part to the local mode frequency appears at 180 cm^{-1}. At high impurity concentration one can therefore define a transverse and a longitudinal part for the local mode $\omega_1^{TO} = 170$ cm^{-1} and $\omega_1^{LO} = 180$ cm^{-1} the calculated value for the local mode frequency is within these limits : $\omega_1 = 167$ cm^{-1} .

Analogous situation has been formed in ZnSe doped with S where the calculated value $\omega_1 = 297$ cm^{-1} is within the limits of that obtained experimentally : $\omega_1^{TO} = 297$ cm^{-1} and $\omega_1^{LO} = 305.5$ cm^{-1}.

Gap modes or band resonances have also been observed in the case of heavy impurities as for example Te in ZnSe where $\omega_g = 182$ cm^{-1} has been deduced from the analysis of the reflectivity spectra.

A quite complete investigation on the effects of heavy doping has been carried in the case of the system CdSe-S. For CdS containing low concentration of Se the dopant acts as a heavy impurity and gives a gap mode at $\omega_g = 180$ cm^{-1}. The increase of the Se concentration brings up two constituants of the ω_g band having respectively the character of a longitudinal ω_g^{LO} and a transverse mode ω_g^{TO}. The frequencies ω_g^{LO} and ω_g^{TO} are linearly dependent on the impurity concentration and tends toward the normal modes frequencies of CdSe at the high concentration limit.

S in CdSe gives two localized modes $\omega_1(\Gamma_1) = 266.5$ cm^{-1} and $\omega_1(\Gamma_5) = 269$ cm^{-1} whose frequencies are also concentrations dependent and reach at high S concentration the normal modes frequencies for CdS.

It seems experimentally that we have a continuous relation between localized and normal modes frequencies depending on concentration. It will be highly interesting to undersee theoretically such a continuous relation when we pass from a perfect lattice to a desordered system.

8. Conclusion.

The discussion of lattice dynamics of II-VI compounds is quite general and interesting in one of the fact that the bonding spanes the whole range from covalent to icnic. A complete calculation of the dispersion relations is now available based on a simple model in which short range forces simulate covalent band contribution and Coulomb forces are functions whose origin is the ionic nature of the bounding. The parameters used in the calculation are plotted with the optically measured normal modes frequencies at the center of the Brillouin zone. The calculated phonon frequencies of the edge of the Brillouin zone in the principal symmetry directions compares well with the experimental values.

Analysis of the coupling of the radiation field with the phonon field is developed in the frame of a macroscopic theory which account well for all the experimental situations. Measurements in blende and wurtzite structures are consistently analysed.

It is shown that numerous arbitrary assignments in the multiphonon optical spectra can be easily erroneous because while it is clear that critical points in the combined density of states give rise to absorption band it is not necessary that this critical point corresponds to critical point in the single phonon density of states. In order to have a critical point in the combined two-phonon density of states the condition $\operatorname{grad} \omega(q) = 0$ can be satisfied also when $\operatorname{grad} \omega(\genfrac{}{}{0pt}{}{q}{j}) = \pm \operatorname{grad} \omega(\genfrac{}{}{0pt}{}{q}{j'})$ which corresponds to equal and opposite of sign slops in the two-phonon branches. It is then clear that the only correct assignments will come from the comparison of the optical absorption spectra with the calculated density of states when the dispersion relations are known. An example concerning CdS is given here.

The introduction of imperfections in the crystal depending on the impurity mass gives rise to localized modes, to resonances or to gap modes. The examen of a certain number of systems has shown that at high impurity concentration the localized as well as the gap modes give rise to a restrahlen band in the reflectivity spectra which submitted to a Kramers-Krönig shows contributions having transverse optical and longitudinal optical characters. With the increase of concentration and forming the ternaryalloys the frequencies of these two parts depart from each other and at about 50% in the concentration reach the values of the normal modes frequencies of the system. This frequency shift seems to be linear with concentration and offers an interesting feature in the study of the transition from perfect crystal with low impurity concentration to the disordered ternary system.

With the development of the investigations of the dispersion relations of perfect crystals we hope to see also further studies concerning the disordered alloys.

REFERENCES

1. H. KAPLAN and J.J. SULLIVAN, Phys. Rev. 130, 120 (1963).

2. J.J. SULLIVAN, J. Phys. Chem. Solids 25, 1039 (1964).

3. L. MERTEN, Z. für Naturforsch 13a, 662, 1067 (1958) ;
                                    15a, 512, 626 (1960) ;
                                    17a, 65, 174, 216 (1962).

4. M.A. NUSIMOVICI and J.L. BIRMAN, Phys. Rev. 156, 925 (1967).

5. T.S. DAMEN, S.P. PORTO and B. TELL, Phys. Rev. 142, 570 (1965).

6. M.A. NUSIMOVICI and J.L. BIRMAN, International Conference on
       II-VI Semiconducting Compounds, Brown University (1967).

7. M. BALKANSKI, J.M. BESSON and R. LE TOULLEC, Proceeding of the
       International Conference on Semiconductors, Paris (1964).

8. R. LE TOULLEC, Thesis, Paris.

9. J.L. BIRMAN, Phys. Rev. 131, 1489 (1963).

10. L. LAX and E. BURSTEIN, Phys. Rev. 97, 39 (1963).

11. M. BORN and M. BLACKMAN, Z. Physik 82, 551 (1933).

12. R.F. WALLIS and A.A. MARADUDIN, Proceedings of the Conference
       of Physics of Semiconductors, Exeter (1962).

13. B. SZIGETTI, Proc. Roy. Soc. A258, 377 (1960).

14. R.F. WALLIS, Phys. Rev. 116, 302 (1959).

15. M. BALKANSKI and W. NAZAREWICZ, J. Phys. Chem. Solids 25, 437
       (1964).

16. W. HAYES, Phys. Rev. 138, A 1227 (1965).

17. S.D. SMITH, R.E.V. Chadock, A.R. GOODWIN, International Confer-
       ence on Semiconductors, Kyoto (1966).

18. A.R. GOODWIN, S.D. SMITH, Phys. Letters 17, 203 (1965).

19. A.J. SIEVERS and STAKENO, Phys. Rev. 140 A 1030 (1965).

20. P.G. DAWBER and R.J. ELLIOTT, Proc. Roy. Soc. A273, 222 (1963).

21. A. MATSUISHI, A. MANABE, H. YOSHINAGA, S. YBUKI and H. KOMIYA,
       Intern. Conf. on Physics of Semiconductors, Kyoto (1966).

22. M. BALKANSKI, R. BESERMAN and L.K. VODOPIANOV, Intern. Conf. on
       Localized Excitation in Solids, Irvine (1967).

23. P. PFEUTY, J.L. BIRMAN, M.A. NUSIMOVICI and M. BALKANSKI, Intern.
       Conf. on Localized Excitation in Solids, Irvine (1967).

24. H.W. VERLEUR and A.S. BARKER Jr., Phys. Rev. 149, 715 (1966) ;
                                               155, 750 (1967).

25. P.G. KLEMENS, Phys. Rev. 122, 443 (1961).

26. R.J. ELLIOTT, W. HAYES, G.D. JONES, H.F. McDONALD, C.T. SENNETT,
       Proc. Roy. Soc. A 289, 1 (1965).

27. A.A. MARADUDIN, Ann. Phys. 30, 371 (1964).

DOCUMENT CONTROL DATA - R & D

(Security classification of title, body of abstract and indexing annotation must be entered when the overall report is classified)

1. ORIGINATING ACTIVITY (Corporate author)	2a. REPORT SECURITY CLASSIFICATION
Laboratoire de Physique des Solides Université de Paris Paris, France	Unclassified
	2b. GROUP

3. REPORT TITLE

OPTICAL STUDIES OF LATTICE VIBRATION IN
II-VI SEMICONDUCTING COMPOUNDS

4. DESCRIPTIVE NOTES (Type of report and inclusive dates)

Scientific.   Interim.

5. AUTHOR(S) (First name, middle initial, last name)

M. Balkanski

6. REPORT DATE	7a. TOTAL NO. OF PAGES	7b. NO. OF REFS
April 2nd 1968	53	27

8a. CONTRACT OR GRANT NO. AF EOOAR-68-0016	9a. ORIGINATOR'S REPORT NUMBER(S)
b. PROJECT NO. 7885	
c. DoD Element 61102F	9b. OTHER REPORT NO(S) (Any other numbers that may be assigned this report)
d. DoD Subelement 681301	ARL 68-0184 U

10. DISTRIBUTION STATEMENT

This document has been approved for public release and sale ; its distribution is unlimited

11. SUPPLEMENTARY NOTES	12. SPONSORING MILITARY ACTIVITY
TECH OTHER	Aerospace Research Laboratories (ARX) Wright-Patterson AFB, Ohio, 45433

13. ABSTRACT

Parallel to the experimental investigations, theoretical studies have been developed and the dispersion relations calculated for some of the II-VI semiconductors compounds.

The presence of foreign atoms leads to localized or resonants modes of vibration, which have been experimentally studied in many II-VI semiconductors compounds.

DD FORM 1 NOV 65 1473

14. KEY WORDS	LINK A		LINK B		LINK C	
	ROLE	WT	ROLE	WT	ROLE	WT
No						

END